

Article

Optimization of Size and Operation of Stand-Alone Renewable-Based Systems with Diesel and Hybrid Pumped Hydro Storage–Battery Storage Considering Uncertainties

Rodolfo Dufo-López * and Juan M. Lujano-Rojas

Department of Electrical Engineering, Universidad de Zaragoza, 50018 Zaragoza, Spain; lujano.juan@unizar.es
* Correspondence: rdufo@unizar.es; Tel.: +34-876555124

Abstract: Currently, the electrical supply in stand-alone systems is usually composed of renewable sources with fossil-fuel generators and battery storage. This study shows a novel model for the metaheuristic–stochastic optimization (minimization of the net present cost, and NPC) of sizing and energy management for stand-alone photovoltaic (PV)–wind–diesel systems with hybrid pumped hydro storage (PHS)–battery storage systems. The model is implemented in C++ programming language. To optimize operations—thus reducing PHS losses and increasing battery lifetimes—optimal energy management can optimize the power limits of using the PHS or battery to supply or store energy. The probabilistic approach considers the variability of wind speed, irradiation, temperature, load, and diesel fuel price inflation. The variable efficiencies of the components and losses and advanced models for battery degradation are considered. This methodology was applied to Graciosa Island (Portugal), showing that, compared with the current system, the optimal system (with a much higher renewable power and a hybrid PHS–battery storage) can reduce the NPC by half, reduce life cycle emissions to 14%, expand renewable penetration to 96%, and reduce the reserve capacity shortage to zero.



Academic Editors: Dongliang Chao and Ottorino Veneri

Received: 13 December 2024

Revised: 15 January 2025

Accepted: 6 February 2025

Published: 8 February 2025

Citation: Dufo-López, R.; Lujano-Rojas, J.M. Optimization of Size and Operation of Stand-Alone Renewable-Based Systems with Diesel and Hybrid Pumped Hydro Storage–Battery Storage Considering Uncertainties. *Batteries* **2025**, *11*, 70. <https://doi.org/10.3390/batteries11020070>

Copyright: © 2025 by the authors. Licensee MDPI, Basel, Switzerland. This article is an open access article distributed under the terms and conditions of the Creative Commons Attribution (CC BY) license (<https://creativecommons.org/licenses/by/4.0/>).

1. Introduction

One of the most important concerns for people living with stand-alone electrical systems (islands or remote regions isolated from the main electrical grid) is energy supply, especially electricity supply [1]. In stand-alone electrical systems, the electrical supply has traditionally been achieved through thermal power plants fed by fossil fuels (gas and diesel) [2]. The electricity supply in these systems usually has a high cost due to the high acquisition cost of some components and high operational costs due to the consumption of diesel, which must be transported to the location. There are also environmental concerns due to emissions from fossil-fuel generators. These systems are particularly vulnerable to energy supply disruptions. Recently, many islands have considered ambitious renewable energy targets, using hybrid renewable minigrids (usually PV, wind, or PV–wind hybrid renewable generation with battery storage and a diesel generator), achieving system reliability, cost savings, and emission reduction [3].

Recently, Fotopoulou et al. [4] reviewed energy storage on non-interconnected European islands, where lithium-ion batteries are the dominant technology, although there are also solutions using PHS and combinations of batteries (Li-ion, lead-acid, nickel chloride,

etc.), supercapacitors, flywheels, and vehicle-to-grid (V2G). In only one case, Madeira (Portugal), a hybrid storage comprising PHS and Li-ion batteries was used (as well as V2G).

On islands and, in general, stand-alone systems, the provision of ancillary services is crucial. Batteries and PHS are suitable technologies for providing ancillary services to non-interconnected power systems, avoiding grid stability problems [4]. Operating reserve requirements have a very important role on islands and must include a reserve constraint, which should be considered in optimizing these systems [5]. Only a few studies regarding the optimization of these systems have included requirements for operating reserves, for example, Schierhorn et al. [6] and Groppi et al. [5]. Traditionally, fossil-fuel generators (typically diesel gensets) run all the time on islands, generating AC voltage and frequency references. In these systems, the maximum allowable penetration of renewable sources is limited for stability reasons (requirements for the minimum load of the gensets). However, for several years, large-scale grid-forming inverters have been used on some islands [7], providing grid voltage and frequency and supplying operating reserves with batteries, achieving high renewable penetration.

Li-ion batteries currently have the highest energy density, power density, roundtrip efficiency, and lifespan [4]. These advantages make Li-ion the most commonly used storage technology in new projects on islands.

PHS is still the dominant electrical energy storage technology in the world, with more than 90% of power and energy storage [8]. PHS is the most mature storage technology, with overall efficiency, long useful life, and rapid response, applicable for voltage stability and frequency control [9]. Rehman et al. [10] presented a technological review of PHS in renewable power systems, showing that it could be the most suitable technology for small islands and mass storage. Javed et al. extensively reviewed solar and wind power generation systems with PHS [9]. Some islands with high renewable penetration, such as El Hierro (Spain) [11], the Faroe Islands [12], and Ikaria (Greece) [13], use PHS for storage. On islands and locations near the sea, PHS can use seawater and the sea itself as lower reservoirs [14].

Depending on the application, the type, and cost of the battery or PHS, PHS can be more cost-effective than batteries, or vice versa. Gioutsos et al. [15] evaluated the optimization of electricity supply on different islands, considering battery storage or PHS. Rodrigues et al. [16] compared PHS and battery storage on Terceira Island (Azores), concluding that using PHS would be more cost-effective. Kotb et al. [17] optimized the hybrid renewable system to supply a reverse-osmosis desalination plant in Egypt, considering flow batteries or PHS, obtaining better results with batteries. Batteries were also found to be the best option in terms of economic benefits and reliability in a case study of Sweden for a PV–wind–storage system optimized by Shabani et al. [18]. Recently, Serat compared PHS and lead–acid battery storage in a PV–hydro stand-alone system in Afghanistan [19], obtaining better economic results using PHS. Katsaprakakis [20] also found better economic results using PHS than using Li-ion battery storage in the electrical supply of rural monasteries in Greece. Ali and Jang [21] optimized the renewable supply of a remote island, obtaining better economic results using PHS than battery storage. Similar conclusions were reached by Alturki and Awwad [22] in the optimization of a renewable system in Saudi Arabia.

Currently, the only PHS–battery system installed on an island is in Madeira (Portugal) [23,24]. Schreider and Bucher [25] showed that PHS–battery storage systems can be a good solution for frequency control, using the battery for the primary reserve due to its fast ramping capability and PHS for the secondary reserve due to its significant autonomy. Several authors have considered the use of hybrid PHS–battery storage systems on islands and, in general, in stand-alone systems. In Greece, Bertsou and Batlas [26] compared hybrid PHS–battery storage systems with other types of storage, obtaining the best results with

hybrid storage. Yadav et al. [27] optimized a PV–wind–PHS–battery microgrid in India by minimizing the levelized cost of energy (LCOE) and considering the charge/discharge limit of the PHS and battery at 15% of the pump’s rated power. Javed et al. [28] used different metaheuristic techniques to optimize the size of a PV–wind–PHS–battery system using 20% of the pump’s rated power for the charge/discharge limit for the PHS and battery. Guezagouz et al. [29] used different metaheuristics to optimize the size of PV–wind–PHS–battery systems using the same charge/discharge 20% limit for the pump’s rated power. Bhayo et al. [30] optimized the size of PV–wind–PHS–battery systems through Particle Swarm Optimization (PSO), using the battery or PHS for the primary power backup (two different strategies). Ma et al. [31] compared a PV–wind system with PHS, battery, or PHS–battery storage but their control strategy for the PHS–battery system was not explained.

Research Gaps and Contributions

The previous studies related to hybrid PHS–battery storage have several limitations. None treat diesel generators as a component of the hybrid system. In all these studies, the authors consider the fixed pump/turbine efficiency, fixed losses in pipelines and fittings, fixed elevation heads, and fixed inverter–charger efficiency. Real variable efficiencies and elevation heads are neglected. Regarding battery aging, only one study related to PHS–battery hybrid storage [29] used a battery degradation model; however, it was a simple model of discharge cycles vs. the depth of discharge, neglecting the effects of the current, state of charge, temperature, etc. The other studies consider a fixed value for the battery lifetime, which can lead to very inaccurate results in many cases. In addition, no previous PHS–battery research has considered operating reserve requirements, which are crucial in stand-alone systems. Furthermore, the operations have not been optimized, and only in a few cases have the authors considered fixed values for the charge/discharge limit of the PHS or battery (15 or 20% of the pump’s rated power). Considering all these simplifications, the optimal systems obtained in previous studies may differ from truly optimal ones.

Regarding the uncertainty of PHS systems, Toufani et al. [32] showed that only a few studies account for uncertainties (the annual variability of wind speed, irradiation, load, etc.) in the optimization of PHS systems. None of the previous optimization studies covering hybrid PHS–battery storage accounted for uncertainties; all of them employed a purely stochastic approach.

Unlike previous research considering hybrid PHS–battery storage, the present study considers the variability of wind speed, irradiation, temperature, load, and diesel fuel price inflation, employing a metaheuristic–stochastic optimization approach. The variable efficiencies of the inverters, pump, and turbine, variable pipeline losses, and variable elevation heads (for the PHS) have also been considered, and an advanced battery degradation and lifetime estimation model is used. To optimize operations, the energy management system optimizes the power limit of the PHS or battery, reducing PHS losses during low power operation and increasing the battery’s lifetime. Variable-speed reversible pump turbines and Li-ion batteries (LFP and LTO) are used in this study.

This study is organized as follows: Section 2 shows the modeling approach for the simulation and system optimization. Section 3 validates the simulation and optimization model. Section 4 presents the computational results and discussion. Finally, Section 5 presents the conclusions.

2. Modeling Approach

The MHOGA software version 4.0 (megawatt hybrid optimization by genetic algorithms, <https://ihoga.unizar.es/en/>), developed by the first author of this study [33], was expanded to include hybrid PHS–battery storage and the other features shown in this study.

The electrical load is supplied through renewable sources and storage and/or a diesel generator; the objective is to minimize the net present cost (NPC) of the system. Maximum unmet load and maximum reserve capacity shortage are the constraints.

The scheme of the photovoltaic–wind–diesel–PHS–battery system is shown in Figure 1.

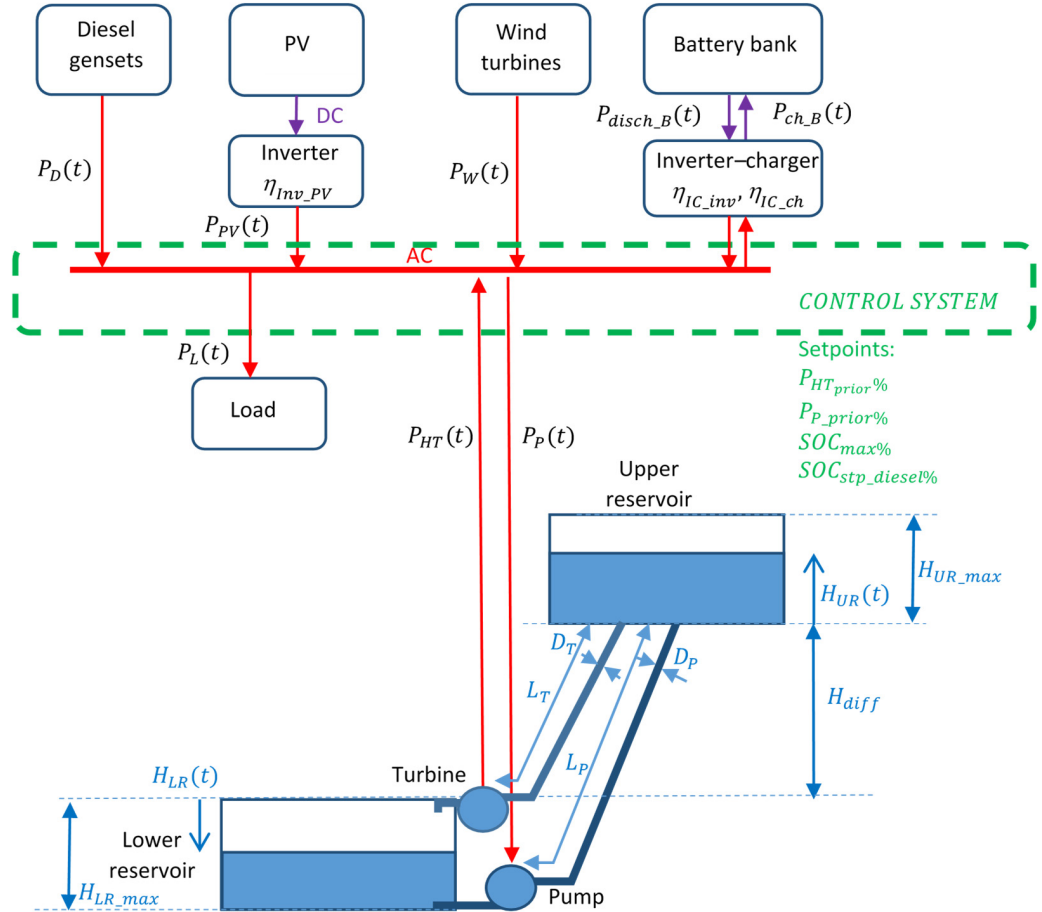


Figure 1. Hybrid system scheme.

The following subsections present the system simulation, the metaheuristic technique, the stochastic approach, and the economic and life cycle emission calculations.

A simulation of each case (a combination of components and setpoints for the control management strategy) is performed over a whole year in 15-min time steps. Different component combinations are considered, as follows: PV generators, wind turbines, diesel gensets, battery banks, PHS systems (pump, turbine, or pump–turbine reversible units and higher and lower reservoirs), and control strategy setpoints (shown below).

For each time step, the net load $P_{Net_load}(t)$ is defined as the load minus the renewable power (Equation (1)):

$$P_{Net_load}(t) = \max(0, P_L(t) - P_{PV}(t) - P_{WT}(t)) \quad (1)$$

where $P_L(t)$, $P_{PV}(t)$, and $P_{WT}(t)$ are, respectively, the load, the power generated by the PV generator, and the power generated by the wind turbines at time t .

The net renewable power is calculated in Equation (2):

$$P_{Net_ren}(t) = \max(0, P_{PV}(t) + P_{WT}(t) - P_L(t)) \quad (2)$$

During each time step t , if there is a net load, it is supplied by the storage (prioritizing the PHS or battery, depending on the strategy). If the storage is empty—that is, the battery

is at the minimum state of charge (SOC) and the PHS upper reservoir is at minimum capacity or they are incapable of supplying the total net load—the remaining net load is supplied by the diesel gensets (which, depending on the control strategy, can charge the battery until a SOC setpoint).

During each time step, if there is net renewable power, it is stored in the PHS or battery, depending on the control strategy.

The setpoints of the control strategy to be optimized are listed below:

- The minimum net load to prioritize the hydro turbine to supply the net load ($P_{HT_prior\%}$) in a percentage of the hydro turbine's rated nominal power (P_{HT_N}): During each time step with the net load, if $P_{Net_load}(t) > P_{HT_prior\%}/100 \cdot P_{HT_N}$, we prioritize the PHS to supply the net load—otherwise, we prioritize the battery. As the hydro turbine efficiency is very low at a low load, optimizing this setpoint will make the turbine run at high efficiency;
- The minimum net renewable power to prioritize the pump to store the net renewable power ($P_{P_prior\%}$) in a percentage of the pump's rated nominal power (P_{P_N}): During each time step with the net renewable power, if $P_{Net_ren}(t) > P_{P_prior\%}/100 \cdot P_{P_N}$, we prioritize the PHS to store energy—otherwise, we prioritize the battery. As the pump efficiency is very low at a low load, optimizing this setpoint will make the pump run at high efficiency;
- Maximum SOC (% of maximum battery capacity) allowed for the battery bank ($SOC_{max\%}$): Li-ion battery degradation increases at a high SOC; by optimizing this setpoint at a value lower than 100%, the degradation will be reduced, and therefore, the lifetime will be extended (but the real capacity to supply the load will be reduced);
- SOC setpoint to charge the battery when the diesel generators are running ($SOC_{stp_diesel\%}$): when the diesel gensets must supply the net load, they will supply the load and charge the battery, working at maximum power (maximum efficiency) until the battery bank setpoint is reached.

2.1. System Simulation

This section estimates renewable power for each time step and demonstrates the performance of the different components.

2.1.1. PV Generator Simulation

The irradiation input data are the global hourly irradiation over the PV's tilted surface, $G(h)$ (W/m^2), for a year. The irradiance in 15-min time steps, $G(t)$ (W/m^2), is obtained using a first-order autoregressive function.

The AC PV generator output (W) during time t is calculated in Equation (3).

$$P_{PV}(t) = \min(\eta_{Inv_PV} P_{PV_N_DC} G(t) / G_{ref} f_{PV_loss} [1 + \alpha / 100 (T_c(t) - T_{c_ref})], P_{Inv_PV_N}) \quad (3)$$

where η_{inv_PV} , $P_{PV_N_DC}$, f_{PV_loss} , α , G_{ref} , T_{c_ref} , $T_c(t)$, and $P_{Inv_PV_N}$ are, respectively, the PV inverter efficiency (which depends on the output inverter power), the rated DC peak power of the PV generator, the efficiency factor (dirt, LV/MV transformer efficiency, wire losses, etc.), the power temperature coefficient ($\%/\text{ }^\circ\text{C}$), the irradiance and cell temperature of standard test conditions (1000 W/m^2 and $25 \text{ }^\circ\text{C}$), the cell temperature ($\text{ }^\circ\text{C}$) during time t , and the output-rated power of the PV inverter (W).

The cell temperature can be estimated with Equation (4):

$$T_c(t) = T_a(t) + \frac{NOCT - 20}{800} G(t) \quad (4)$$

where $T_a(t)$ ($^{\circ}\text{C}$) is the ambient temperature; and NOCT ($^{\circ}\text{C}$) is the nominal operation cell temperature.

2.1.2. Wind Turbine Simulation

Hourly wind speed data at the wind turbine hub height for an entire year are used as the input. The wind speed for each 15-min time step was obtained similarly to the irradiation data (first-order autoregressive model). The wind turbine output power curve is measured under standard conditions (air density, $\rho_{air_0} = 1.225 \text{ kg/m}^3$). Air density depends on temperature and air pressure; for each time step, if the air density, $\rho_{air}(t)$ (kg/m^3), is different from the standard, the wind turbine output curve is converted by multiplying by the ratio $\rho_{air}(t)/\rho_{air_0}$.

The wind turbines with pitch control maintain their nominal power (P_{WT_N}) without any changes, as shown in Figure 2. The wind turbine output power, $P_{WT}(ws, t)$ (W), at time t for each wind speed, $ws(t)$ —lower than the rated wind speed (ws_{rated} , Figure 2: 16 m/s)—is outlined below:

$$P_{WT}(ws, t) = P_{WT_{curve}}(ws)\rho_{air}(t)/\rho_{air_0}f_{WT_loss} \quad \forall ws < ws_{rated} \quad (5)$$

where $P_{WT_{curve}}(ws)$ represents the wind turbine output power curve under standard conditions; and f_{WT_loss} is the efficiency owing to losses in LV/HV transformers, wires, switches, etc.

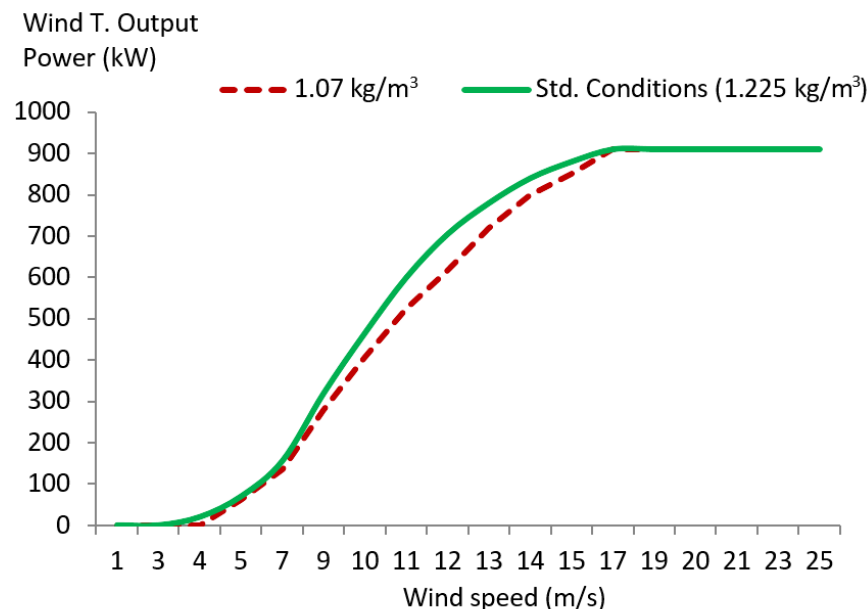


Figure 2. A 900 kW wind turbine output curve with pitch control. Output curve conversion by multiplying by the ratio $\rho_{air}(t)/\rho_{air_0}$.

The wake effect model [34] is used to calculate the total output power of the wind park.

2.1.3. Battery Simulation and Aging Model

Li-ion batteries include several advantages such as high energy and power density, a high cycle life, availability to supply high power (several times their energy capacity), a high response speed, and no maintenance needs, among others, making them ideal for islands. Among the different Li-ion technologies [35], in this study, we consider the lithium titanate (LTO) and the lithium iron phosphate (LFP) types. LFP batteries are typical in stand-alone systems due to their good cycle life, low cost (compared with LTO), and low

fire risk [36]. On the other hand, LTO batteries have the advantages of ultrafast discharge and charge rates and much higher life cycles (as much as 5 times higher than LFP batteries).

The battery's charge and discharge power are limited by their maximum allowed values, $P_{B_ch_max}$ and $P_{B_disch_max}$ (considering its maximum C-rates), and by the SOC.

$$P_{B_ch}(t) = \min\left(P_{B_ch}(t), P_{B_ch_max}, \frac{SOC_{max} - SOC(t)}{\eta_{B_ch}\Delta t}\right) \quad (6)$$

$$P_{B_disch}(t) = \min\left(P_{B_disch}(t), P_{B_disch_max}, \frac{SOC(t) - SOC_{min}}{\Delta t}\eta_{B_disch}\right) \quad (7)$$

where $SOC(t)$ (Wh) is the state of charge at the beginning of time t ; SOC_{max} and SOC_{min} (Wh) are the maximum and minimum allowed SOC values; η_{B_ch} and η_{B_disch} are the charge and discharge efficiencies; and Δt (h) is the duration of the time step (in this study, 0.25 h). SOC_{max} is the nominal capacity of the battery (C_B) multiplied by the control variable $SOC_{max\%}/100$.

The inverter–charger (battery inverter) efficiency is taken into account. In the charge process, the charge power from the AC bus (from the renewable sources or from the diesel genset) is higher than $P_{B_ch}(t)$ in the ratio $1/\eta_{IC_ch}$. In the discharge process, the discharge power injected into the AC bus (to supply net load) is lower than $P_{B_disch}(t)$ in the ratio η_{IC_inv} , where η_{IC_ch} and η_{IC_inv} are the inverter–charger variable efficiencies in the charger mode and in the inverter mode, respectively.

The SOC at the beginning of the next time step ($t + 1$) is calculated using Equation (8) if a charge or discharge is applied (if there is no charge or discharge current, a self-discharge rate is applied).

$$SOC(t + 1) = SOC(t) + P_{B_ch}(t)\Delta t\eta_{B_ch} - \frac{P_{B_disch}(t)}{\eta_{B_disch}}\Delta t \quad (8)$$

LFP cycle aging [37] and calendar aging [38] models designed by Naumann et al. are used in this study. Capacity fading is a combination of cycle and calendar aging. Cycle aging is the percentage of capacity loss due to cycling (Q_{loss_cyc} (%), Equation (9)), which depends on the full equivalent cycles (FECs) performed, the depth of discharge (DOD), and the charge/discharge rate. Calendar aging can be estimated as the percentage of capacity loss due to the calendar (Q_{loss_cal} (%), Equation (10)), depending on temperature, the SOC, and time.

$$Q_{loss_cyc} = \sum_{i=1}^{10} (a_{cyc}C_{rate} + b_{cyc}) \left((DOD_i - 0.6)^3 c_{cyc} + d_{cyc} \right) FEC_i^z \quad (9)$$

$$Q_{loss_cal} = k_{ref} \exp\left(\frac{-E_a}{R} \left(\frac{1}{T_{aver}} - \frac{1}{T_{ref}}\right)\right) \left((SOC_{aver} - 0.5)^3 c_{cal} + d_{cal} \right) \sqrt{60t_{bat}} \quad (10)$$

where FEC_i is the number of full equivalent cycles counted in $i = 10$ different intervals of the depth of discharge DOD_i ; C_{rate} is the average discharge C-rate of each interval; t_{bat} (min) is the time that has passed with an average charge level, SOC_{aver} (per unit), and average temperature, T_{aver} (K); E_a is the activation energy ($17,126 \text{ Jmol}^{-1}$); $R = 8.314 \text{ Jmol}^{-1}\text{K}^{-1}$ is the universal gas constant; T_{ref} is the reference temperature (298.15 K); and k_{ref} , a , b , c , d , and z are constant parameters [37,38] that can be modified to fit the aging performance of another manufacturer's battery.

Regarding LTO degradation, the data for some constant parameters are modified to fit the capacity loss results obtained by Stroe et al. [39]: $c_{cyc} = 2.4$ and $d_{cyc} = 1$.

A maximum operating life of 20 years is considered for both the LFP and LTO batteries, as usual for stationary batteries [38].

2.1.4. PHS Simulation

Variable-speed pumps are used in this study (reversible pump–turbine or a pump unit different from the turbine unit). Mousavi et al. [40] calculated the flow rate of the pump, $Q_P(t)$ (m^3/s), depending on the input power $P_P(t)$, the pump efficiency $\eta_P(t)$, and the pump head $H_P(t)$ (m). The flow rate cannot be higher than the nominal (Q_{P_N}). In addition, at the end of the time step ($\Delta t_S = 15 \cdot 60 = 900$ s), the water stored in the lower reservoir, $V_{LR}(t)$ (m^3), cannot be lower than its allowed minimum, V_{LR_min} (m^3), and the upper reservoir water volume, $V_{UR}(t)$ (m^3), cannot be higher than its allowed maximum, V_{UR_max} (m^3).

$$Q_P(t) = \min\left(\frac{P_P(t)\eta_P(t)}{\rho g H_P(t)}, Q_{P_N}, \frac{V_{LR}(t) - V_{LR_min}}{\Delta t_S}, \frac{V_{UR_max} - V_{UR}(t)}{\Delta t_S}\right) \quad (11)$$

where ρ is the water density (Kg/m^3); g is the gravity acceleration (m/s^2); and $H_P(t)$ (m) is the total pump head (static head $H_{PS}(t)$ plus head loss $H_{Pl}(t)$).

$$H_P(t) = H_{PS}(t) + H_{Pl}(t) \quad (12)$$

The static head is calculated in the following equation (see Figure 1):

$$H_{PS}(t) = H_{diff} + H_{UR}(t) + H_{LR}(t) \quad (13)$$

where $H_{UR}(t)$ and $H_{LR}(t)$ are calculated at each time step t , knowing the upper and lower volume ($V_{UR}(t)$ and $V_{LR}(t)$), their maximum capacities (V_{UR_max} and V_{LR_max}), and reservoir depths (H_{UR_max} and H_{LR_max}) and assuming they are parallelepiped shaped.

The head loss, $H_{Pl}(t)$, is due to water friction in the pipelines and fittings. Thus, the Darcy–Weisbach equation [40] is used (Equation (14)).

$$H_{Pl}(t) = K \frac{v(t)^2}{2g} \quad (14)$$

$$v(t) = \frac{Q_P(t)}{0.25\pi D_P^2} \quad (15)$$

$$K = K_{pipe} + K_{fittings} \quad (16)$$

$$K_{pipe} = f \frac{L_P}{D_P} \quad (17)$$

Under turbulent flow (common in PHS systems), the Haaland approximation for the Colebrook equation is used as follows:

$$f = \left[-1.8 \log \left(\frac{6.9}{Re(t)} + \left(\frac{\varepsilon/D_P}{3.7} \right)^{1.11} \right) \right]^{-2} \quad (18)$$

where K , K_{pipe} , $K_{fittings}$, $v(t)$, D_P , L_P , ε , and $Re(t)$ are, respectively, the total resistance coefficient, pipe resistance coefficient, fittings resistance coefficient, water speed (m/s), pipe diameter and length (m), absolute roughness (m), and Reynolds number (which depends on the pipe diameter, water speed, and dynamic viscosity and is > 2300 for turbulent flow).

The hydro turbine output power, $P_{HT}(t)$ (W), which the turbine must supply depends on the control strategy, the renewable power, and the load. It is limited by P_{HT_N} (W), the nominal flow rate Q_{HT_N} (m^3/s), and the water reservoir volume.

$$P_{HT}(t) = \min\left(P_{HT}(t), P_{HT_N}, \min\left(Q_{HT_N}, \frac{V_{LR_max} - V_{LR}(t)}{\Delta t_S}, \frac{V_{UR}(t) - V_{UR_min}}{\Delta t_S}\right) \rho g H_{HT}(t) \eta_{HT}(t)\right) \quad (19)$$

Mousavi et al. [40] calculated the flow rate of the turbine, $Q_{HT}(t)$ (m^3/s), depending on the output power and water reservoir volume:

$$Q_{HT}(t) = \min\left(\frac{P_{HT}(t)}{\rho g H_{HT}(t) \eta_{HT}(t)}, Q_{HT_N}, \frac{V_{LR_max} - V_{LR}(t)}{\Delta t_S}, \frac{V_{UR}(t) - V_{UR_min}}{\Delta t_S}\right) \quad (20)$$

where $\eta_{HT}(t)$ is the turbine efficiency (which depends on the water flow); and $H_{HT}(t)$ (m) is the turbine head (static head in turbine mode, $H_{TS}(t)$ minus the head loss, $H_{HTl}(t)$, Equation (21)).

$$H_{HT}(t) = H_{TS}(t) - H_{HTl}(t) \quad (21)$$

The static turbine head is calculated in Equation (22) (see Figure 1).

$$H_{TS}(t) = H_{diff} + H_{UR}(t) \quad (22)$$

In the case of considering a single-pump–turbine reversible unit, the height $H_{LR}(t)$ would have to be added to that height (obtaining Equation (13)).

The head loss is calculated using the same equations as those for the loss in pump mode using $Q_{HT}(t)$, turbine pipe data (diameter D_{HT} and length L_{HT}), and the fittings.

2.1.5. Diesel Genset Simulation

Several diesel gensets can be present in a system, running the number needed to meet the net load in parallel (when the control strategy determines that the diesel genset must supply power). The diesel genset output power of each unit, $P_D(t)$ (kW), depends on the output power of the renewable sources, the load, the control strategy, and the number of diesel gensets that are running. The diesel fuel consumption (L/h) of each unit during time step t is considered as follows.

If the unit was running during the previous time step (Equation (23)),

$$Cons_{fuel}(t) = A \cdot P_{D_N} + B \cdot P_D(t) \quad (23)$$

If the unit was not running during the previous time step (Equation (24)),

$$Cons_{fuel}(t) = [A \cdot P_{D_N} + B \cdot P_D(t)](1 + F_{start}) \quad (24)$$

where $A = 0.246 \text{ L/kWh}$ and $B = 0.08415 \text{ L/kWh}$ are the fuel curve coefficients [41,42]; P_{D_N} (kW) is the diesel genset rated power; and F_{start} is a factor considering the extra fuel due to the start. To avoid excessive starts and stops, a minimum running time (1 h in this study) is applied to each diesel genset unit.

2.2. Metaheuristic–Stochastic Optimization

Due to the nonlinear characteristics of some components (the PV inverter and inverter-charger efficiencies, wind turbine output curve, pump–turbine efficiency, pipeline losses, etc.), optimization cannot be performed with classical methods or MILP. Thus, the genetic algorithm (GA) metaheuristic technique was used for the optimization. The uncertainties will be considered using a stochastic approach (Monte Carlo simulation, MCS).

GAs have been widely used in the optimization of hybrid renewable systems. In the review by Akbas et al. [43], GAs were identified as the most common metaheuristic technique for optimizing such systems, while the second most popular technique was Particle Swarm Optimization (PSO).

2.2.1. Metaheuristic Optimization Using GAs

Two GAs were considered in the optimization: a main algorithm to determine an optimal configuration of the components, and a secondary algorithm to obtain optimal control (Figure 3). Furthermore, the simulation of each combination of components and control strategies considered by the GA is repeated $MCS_{samples}$ times (the MCS approach), using probability density function (PDF) curves for the data and obtaining PDFs for the results (Figure 3).

Main GA (optimize components)

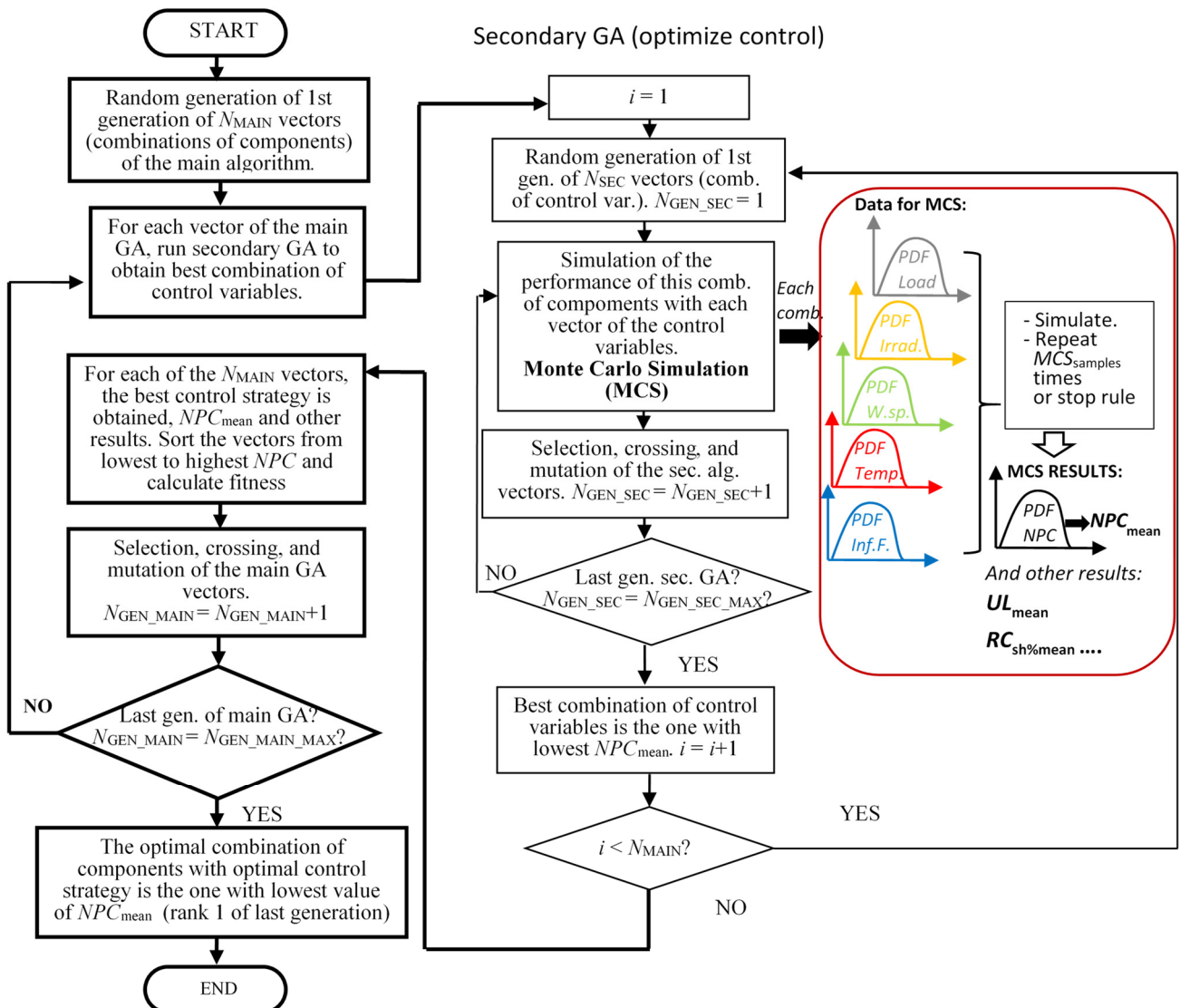


Figure 3. Metaheuristic–stochastic optimization: two GAs (main and secondary), including MCS.

Up to ten variables can be optimized with the main GA (Equation (25)):

$$\{PV_{type}, N_{PV}, WT_{type}, N_{WT}, D_{type}, N_D, B_{type}, N_B, PHS_{type}, PHS_{dur}\} \quad (25)$$

where PV_{type} , WT_{type} , D_{type} , B_{type} , and PHS_{type} are, respectively, the different types (technologies and/or sizes) of PV, wind turbines, diesel generators, batteries, and pump–turbine reversible units (or different pump and turbine machines) considered. N_{PV} , N_{WT} , N_D , and N_B are their numbers in parallel. PHS_{dur} (h) is the duration of the upper reservoir at the turbine’s rated flow. In this study, we consider the inverter–charger to be fixed (non-optimizable).

The secondary GA optimizes the control strategy (for each combination of the main GA), which can be composed of up to four setpoint variables (explained in Section 2), as per Equation (26).

$$\left| P_{HT_prior\%}, P_{P_prior\%}, SOC_{max\%}, SOC_{stp_diesel\%} \right| \quad (26)$$

The key mechanisms of GA are natural selection, recombination (crossover), and mutation (change in the genes) [28]. The first mechanism involves selecting parents randomly to create a new child for the next generation using the roulette wheel method [28] outlined in this study. The crossover operator recombines the selected parents, and new children are created, from which the next generation is selected. Mutation is used to enhance the exploration by randomly selecting a variable (gene) of a child to mutate.

The objective of the optimization is to find a combination of components and a control strategy that minimizes the NPC_{mean} (the mean of the probability distribution curve of the NPC results of the different simulations obtained with the MCS: each combination is simulated $MCS_{samples}$ times). The NPC result of each combination is a PDF, from which the mean value (NPC_{mean}) is considered by the objective function of the GA (Equation (27)).

$$\min(NPC_{mean}) \quad (27)$$

The following constraints must be met:

- The mean of the unmet load, UL_{mean} (%) (mean value of the PDF of the UL results of each combination), must be lower than the maximum unmet load allowed (UL_{max}):

$$UL_{mean} < UL_{max} \quad (28)$$

- The total reserve capacity shortage, $RC_{sh\%mean}$ (% of total load) (mean value of the PDF of the $RC_{sh\%}$ results), must be lower than the maximum allowed, $RC_{sh_max\%}$ (%):

$$RC_{sh\%mean} < RC_{sh_max\%} \quad (29)$$

The $RC_{sh\%}$ of each MCS is obtained as follows (Equation (30)):

$$RC_{sh\%} = \frac{\sum_t RC_{sh}(t)}{\sum_t P_L(t)(t)} \cdot 100 \quad (30)$$

where $RC_{sh}(t)$ (Equation (31)) is the reserve capacity shortage of each time step. This is calculated as the operating reserve required by the load plus the PV generation plus the wind turbine generation minus the real reserve supplied by the battery, the number of diesel generators running in that time step, and the hydro turbine if it is supplying power in that time step.

$$\begin{aligned}
RC_{sh}(t) = \max & (0, P_L(t)RR_L + P_{PV}(t)RR_{PV} + P_{WT}(t)RR_{WT} \\
& - \left(\min(P_{B_disch_max}, \frac{(SOC(t) - SOC_{min})\eta_{B_disch}}{\Delta t_{RES}}) \right. \\
& + \sum_{N_{D_run}(t)} (P_{D_N} - P_D(t)) \\
& \left. + \min((P_{HT_N} - P_{HT}(t)), \min(Q_{HT_N}, \frac{V_{LR_max} - V_{LR}(t)}{\Delta t_{RES} \cdot 3600}) \rho g H_{HT}(t) \eta_{HT}(t)) \right)
\end{aligned} \tag{31}$$

where RR_L , RR_{PV} , and RR_{WT} are the operating reserve requirements for load, PV, and wind power; $N_{D_run}(t)$ is the number of diesel generators running during this time step t ; and Δt_{RES} (h) is the time the battery and PHS require to supply the reserve capacity. If $RC_{sh}(t) > 0$ during this time step, the hydro turbine runs at its minimum power to increase reserve capacity; if this is not enough, the necessary diesel units will start to reduce reserve capacity shortage to zero.

Different authors have considered different reserve requirements. Schierhorn et al. [6] considered an operating reserve requirement of 10% of the load ($RR_L = 0.1$) plus 80% solar output ($RR_{PV} = 0.8$), while Groppi et al. [5] considered a requirement operating reserve of 10% for load and 20% for the PV and wind power ($RR_L = 0.1$; $RR_{PV} = RR_{WT} = 0.2$).

2.2.2. Stochastic Approach

The secondary GA optimizes the control variables and includes the MCS. Usually, the annual irradiation, annual average wind speed, annual average temperature, and annual load vary from year to year such that their probability density functions (PDFs) approximately follow normal or Gaussian curve distributions. The MCS repeats the simulation of each component and control strategy combination a specific number of times ($MCS_{samples}$), using random values for the inputs each time (load, irradiation, temperature, wind speed, and diesel fuel price inflation). These follow a Gaussian curve distribution (which considers their correlations). The results for the $MCS_{samples}$ (NPC, LCOE, unmet load, reserve capacity shortage, energy supplied by the different components, etc.) are represented in PDF distributions.

The MCS procedure applied is explained below.

The data for the MCS (Figure 3) are the Gaussian probability density functions (PDFs) of the annual load, irradiation, temperature, and wind speed, which are usually correlated variables. Their variance–covariance matrix is known. In addition, the Gaussian PDF of the annual diesel fuel price interest rate are data for the MCS.

For each sample ($MCS_{samples}$) of each component and control strategy combination, a random vector of correlated Gaussian random variables, Z (composed of load, L; irradiation, G; temperature, T; and wind speed, W), is obtained.

$$Z = \begin{pmatrix} L \\ G \\ T \\ W \end{pmatrix}; Z \sim N(\mu, \Sigma) \tag{32}$$

where μ is the mean values vector of the PDF Gaussian distributions of the annual load, irradiation, temperature, and wind speed; and Σ is the variance–covariance matrix (symmetrical) [44,45].

$$\mu = \begin{bmatrix} L_{mean} \\ G_{mean} \\ T_{mean} \\ W_{mean} \end{bmatrix}; \Sigma = \begin{bmatrix} var(L) & cov(L, G) & cov(L, T) & cov(L, W) \\ cov(G, L) & var(G) & cov(G, T) & cov(G, W) \\ cov(T, L) & cov(T, G) & var(T) & cov(T, W) \\ cov(W, L) & cov(W, G) & cov(W, T) & var(W) \end{bmatrix} \tag{33}$$

The procedure shown below ([46]) is repeated $MCS_{samples}$ times or until the stopping rule of the MCS is reached:

- (i) A vector, \mathbf{X} (the same size as \mathbf{Z}), is generated, which is distributed with a standard normal distribution considering that \mathbf{I} is an appropriately sized identity matrix:

$$\mathbf{X} \sim N(0, \mathbf{I}) \quad (34)$$

- (ii) The vector of the correlated Gaussian random variables is obtained using the following expression:

$$\mathbf{Z} = \mathbf{C}\mathbf{X} + \boldsymbol{\mu} \quad (35)$$

where \mathbf{C} is the Cholesky factor (lower triangular matrix) of the variance–covariance matrix ($\mathbf{CC}' = \Sigma$). In addition, a random value of the diesel fuel price inflation is obtained from its Gaussian PDF;

- (iii) A new annual time series of load, irradiation, temperature, and wind speed is obtained from the original time series, applying a random variation to the value of each time series ($\pm R_{var}$ (%)) so that the average values of the new series are the values of vector \mathbf{Z} , that is, L, G, T, and W, respectively (obtained in step (ii));
- (iv) The performance of the system over a year is simulated using the time series obtained in step (iii). NPC and other results are calculated considering the random diesel price inflation obtained in step (ii).

The procedure (i–iv) is repeated for the sample size of the MCS ($MCS_{samples}$) times or until the stopping rule of the MCS is reached. All the results are obtained as PDF distribution curves. As noted, the PDF mean of the NPC is the value NPC_{mean} , which uses the GAs (secondary and main) to evaluate the fitness of the component and control strategy combination. The stopping rule [45] makes the MCS stop when the relative standard error of the NPC reaches a specified value, $RSE\%$ (Equation (36)).

$$\frac{\frac{NPC_{SD}}{\sqrt{n}}}{NPC_{mean}} \cdot 100 < RSE\% \quad (36)$$

where NPC_{SD} is the standard deviation of the PDF of the NPC results obtained up to the moment; and n is the number of samples evaluated.

2.3. Economics

For each component and control strategy combination, the NPC (EUR) is calculated for each MCS sample. This includes the capital expenditures ($CAPEX_j$), the annual operational expenditures ($OPEX_j$), and the net present cost of the replacements (NPC_{rep_j}) during the lifetime of the system for all components, j . It also includes the annual operation and maintenance costs of the diesel (including fuel costs), $OPEX_D$.

$$NPC = \sum_j \left(CAPEX_j + NPC_{rep_j} + \sum_{y=1}^Y \left(OPEX_j \frac{(1+Inf)^y}{(1+I)^y} \right) + \sum_{y=1}^Y \left(OPEX_D \frac{(1+Inf_{fuel})^y}{(1+I)^y} \right) \right) \quad (37)$$

where Y is the system lifetime (years); I is the annual nominal discount rate; Inf is the annual general inflation rate; and Inf_{fuel} is the diesel fuel inflation rate, which is one of the PDF input variables.

The leveled cost of energy, $LCOE$ (EUR/kWh), is the cost per kWh of load.

$$LCOE = \frac{NPC \cdot CRF}{E_{load}} \quad (38)$$

where E_{load} (kWh/yr) is the total annual load consumption. CRF is the capital recovery factor (Equation (39)).

$$CRF = \frac{r(1+r)^N}{(1+r)^N - 1} \quad (39)$$

where r is the annual real discount rate.

$$r = \frac{I - Inf}{1 + Inf} \quad (40)$$

2.4. Life Cycle Emissions

Life cycle emissions, LCE (equivalent kg of CO₂ emissions during the system lifetime, kg CO₂-eq), can be calculated by adding the equivalent CO₂ emissions of component manufacturing, transport, installation, and recycling, and the emissions due to diesel fuel consumption over the system's lifetime.

$$LCE = P_{PV_N_DC} \cdot N_{PV} \cdot Em_{PV/kW} + P_{WT_N} \cdot N_W \cdot Em_{WT/kW} + C_B \cdot N_B \cdot Em_{B/kWh} + E_{T_year} \cdot Y \cdot Em_{PHS/kWh} + Cons_{D_year} \cdot Y \cdot Em_{D/L} \quad (41)$$

where $Em_{PV/kW}$ and $Em_{WT/kW}$ (kg CO₂-eq/kW) are the life cycle emissions per kW of rated power of the PV generator and the wind turbine, respectively; $Em_{B/kWh}$ (kg CO₂-eq/kWh) is the life cycle emissions per kWh of battery capacity (C_B); $Em_{PHS/kWh}$ (kg CO₂-eq/kWh) is the life cycle emissions per kWh of energy supplied by the PHS turbine; $Em_{D/L}$ (kg CO₂-eq/L) is the emissions per liter consumed by the diesel generator; E_{T_year} (kWh/yr) is the energy supplied by the PHS turbine over one year; and $Cons_{D_year}$ (L/yr) is the diesel fuel consumption of all the diesel gensets over one year.

2.5. Statistical Analysis of Optimization Techniques

Four statistical parameters are defined to evaluate the performance and stability of the optimization techniques [28]: standard deviation (SD_{opt}), mean absolute error (MAE_{opt}), relative error (RLE_{opt}), root mean square error ($RMSE_{opt}$), and mean efficiency (η_{opt}). The optimization technique is executed a specific number of times (R) and the objective function values (NPC_{mean}) from the different runs are used to calculate the statistical parameters.

$$SD_{opt} = \sqrt{\frac{1}{R-1} \sum_{r=1}^R (x_r - \bar{x})^2} \quad (42)$$

where $x_r = NPC_{mean}$ is the objective function value at the r th run; and \bar{x} is the mean of the R runs.

$$MAE_{opt} = \frac{\sum_{r=1}^R (x_r - x_{min})}{R} \quad (43)$$

where x_{min} is the minimum of the objective function value obtained in R runs.

$$RLE_{opt} = \frac{\sum_{r=1}^R (x_r - x_{min})}{x_{min}} \quad (44)$$

$$RMSE_{opt} = \sqrt{\frac{1}{R} \sum_{r=1}^R (x_r - x_{min})^2} \quad (45)$$

$$\eta_{opt} = \frac{\sum_{r=1}^R \left(100 \frac{x_{min}}{x_r} \right)}{R} \quad (46)$$

All statistical results are expressed in the same unit as the objective function, except for RLE_{opt} (dimensionless) and η_{opt} (%).

3. Validation of the Model

To validate the simulation and optimization model presented in Section 2, the optimization results obtained by Javed et al. [28]—who used different metaheuristic techniques—were compared with those obtained in our study. Javed et al. [28] performed the deterministic optimization of a PV–wind renewable system with hybrid PHS–battery storage to supply the load (256 kWh/day average, and peak 31 kW) of a small island near Shanghai. However, this study has several limitations: it is deterministic, assumes a fixed battery lifetime, and uses fixed efficiencies and losses. As shown in the introduction, there is no previous research similar to ours, as all prior studies share the same limitations as those of Javed et al.

In our study, hourly load data were estimated from the data provided by Javed et al. [28]; some data were missing in that reference, such as the wind turbine power curve (assumed to be a commercial 5 kW unit), hub height (assumed as 10 m), inverter–charger efficiency (assumed fixed values of $\eta_{IC_ch} = \eta_{IC_inv} = 95\%$), PV inverter power (assumed to be the same as PV-rated power), efficiency (assumed fixed value $\eta_{inv_PV} = 95\%$), and other data related to losses (assumed as $f_{PV_loss} = 0.95$, NOCT = 43 °C, and $\alpha = -0.4\%/\text{°C}$). Hourly irradiation (14° slope, south-oriented), ambient temperature, and wind speed at hub height data were downloaded from the Renewables Ninja [47] database, while Javed et al. [28] used in situ measured data. Deterministic optimization (without MCS) was performed, with 0% unmet load allowed. The following components were considered in our research: PV of 1 kW, from 0 to 200 in parallel; wind turbines of 5 kW, from 0 to 20 in parallel; a 5 kWh battery, from 0 to 200; PHS of 31 kW, with the reservoir duration in steps of 1 h, from 1 to 32 h (while Javed et al. considered 1000 steps); and an inverter–charger of 31 kW. Control variables were not considered for the optimization; Javed et al. [28] used a fixed value of 20% for $P_{HT_prior\%}$ and for $P_{P_prior\%}$, $SOC_{max\%} = 100\%$ and $SOC_{stp_diesel\%}$ was not considered as there was no diesel genset.

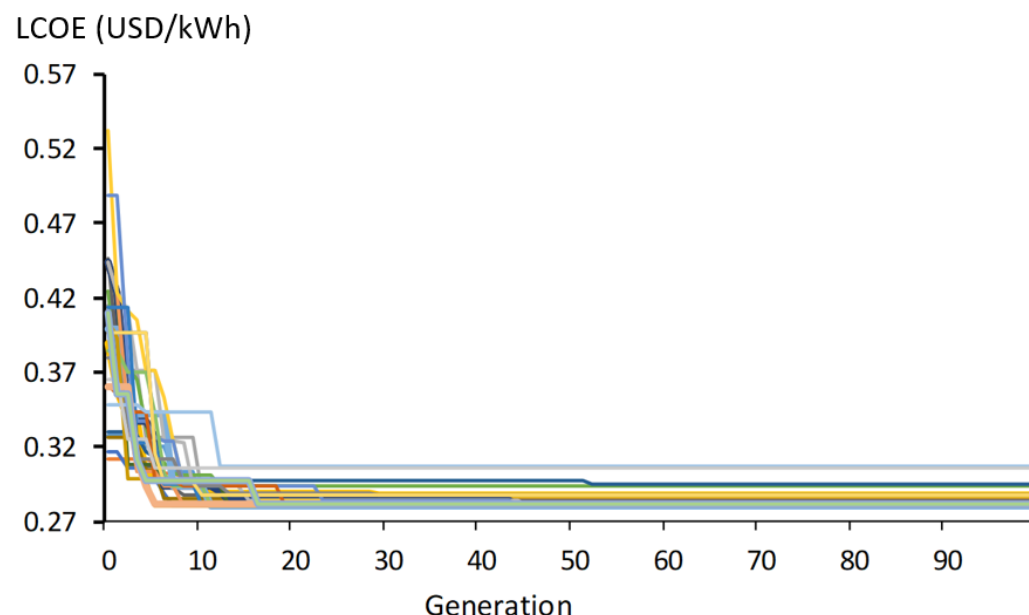
The number of possible combinations of component types and quantities in parallel is $1 \times 201 \times 1 \times 21 \times 1 \times 201 \times 32 = 27.15$ million. The computation speed of the computer is 40 simulations (1-h time steps over a whole year) per second; therefore, evaluating all the components took 4 days and 3 h to obtain the global optimum. Using the GA with the same parameters as Javed et al. [28] ($N_{GEN_MAIN_MAX} = 100$; $N_{MAIN} = 100$; crossover rate 90%; and mutation rate 1%), the optimization took less than 4 min. The optimization was repeated $R = 30$ times.

The results are compared in Table 1. The first four rows show the range of the components' sizes for the optimal results found from the 30 executions. Javed et al. [28] calculate LCOE (they call it cost of energy, COE) as shown in Equation (38), which is shown in the fifth row of Table 1. The last six rows present the statistical parameters for the metaheuristic techniques (note that the GA of Javed et al. was not as effective because, in our case, the variable of the PHS reservoir duration considers 32 possible values, while they considered 1000 steps) and the average execution time (note that the GA used by Javed et al. was significantly slower, by a factor of 100, because they implemented it in Matlab (<https://www.mathworks.com/products/matlab.html>), whereas our research utilizes C++).

Table 1. Results compared with those of Javed et al. [28].

Variable	Javed et al. [28], GA	This Study
PV (kW)	90–93	103–119
Number of WTs (5 kW)	14–15	10–11
Upper reservoir duration (h)	8.9–9	6–8
Battery (kWh)	56–58	61–79
$LCOE$ (USD/kWh)	0.244–0.2599	0.2799–0.3067
SD_{opt} (USD/kWh)	0.0033	0.0071
RLE_{opt}	0.8779	0.471
MAE_{opt} (USD/kWh)	0.0071	0.0042
$RMSE_{opt}$ (USD/kWh)	0.0112	0.0082
η_{opt} (%)	93.93	95.33
Average execution time (in minutes)	420	3.9

The evolution of the COE over the generations of the GA is shown in Figure 4 (thirty curves, one for each execution of the optimization). In total, 22 out of the 30 runs obtained the global optimum.

**Figure 4.** Evolution of the COE, with each color representing one of the thirty runs.

Considering the assumptions made due to the missing data in the original study, the model presented in Section 2 is validated. In addition, it was found that the calculation speed is more than 100 times faster than that of previous research. This higher speed allows the stochastic optimization to be performed in a similar amount of time as other studies using deterministic optimization.

4. Results and Discussion

The simulation and optimization model presented in Section 2 were used to optimize the generation system of Graciosa Island (Azores, Portugal). This island was selected because its current generation system (a PV–wind–diesel–battery system) has been detailed in several publications [48–50] allowing for a comparison of the real performance of the current system with the results obtained in this study. Additionally, there are elevation differences on the island that make it suitable for including PHS in the generation system. Graciosa Island has an area of 60.65 km², a length of 10 km, and a width of 7 km. The population is 4091.

First, the performance of the island's current generation system is simulated and compared with real data. Then, the optimization of the hybrid system (including hybrid PHS–battery storage) is carried out, first deterministically and later stochastically.

4.1. Simulation of the Current Generation System of Graciosa Island

The performance of the current energy system of Graciosa Island was simulated using a deterministic approach, and the results were compared with the real data provided by the island operator, Greensmith Energy Management System (GEMS) [48].

Graciosa Island's hybrid system comprises the following [48–50]:

- A 4.6 MW diesel power plant ($3 \times 600, 1 \times 810, 2 \times 1000$ kW) with a minimum of 30% load for each unit;
- A 4.5 MW wind farm (5×900 kW WTs, 55 m hub height);
- A 1 MW_{DC} PV power plant (4000 modules $\times 250$ Wp);
- A 3.2 MWh/6 MW LTO battery energy storage system (40 racks of 19 modules with 60 cells each) with a SOC minimum of 30%;
- A 7.425 MW inverter–charger (3×2.475 MW). Grid-forming inverters with black start capability are used [7].

Hourly irradiation (30° slope, south-oriented) and ambient temperature data are downloaded from the PVGIS [51] database (which provides accurate data for Europe). The wind speed at hub height is downloaded from the Renewables Ninja [47] database. The downloaded data are for 2019. The load time series in 15-min time steps over the year is estimated from [48–50]. Figure 5 shows the data.

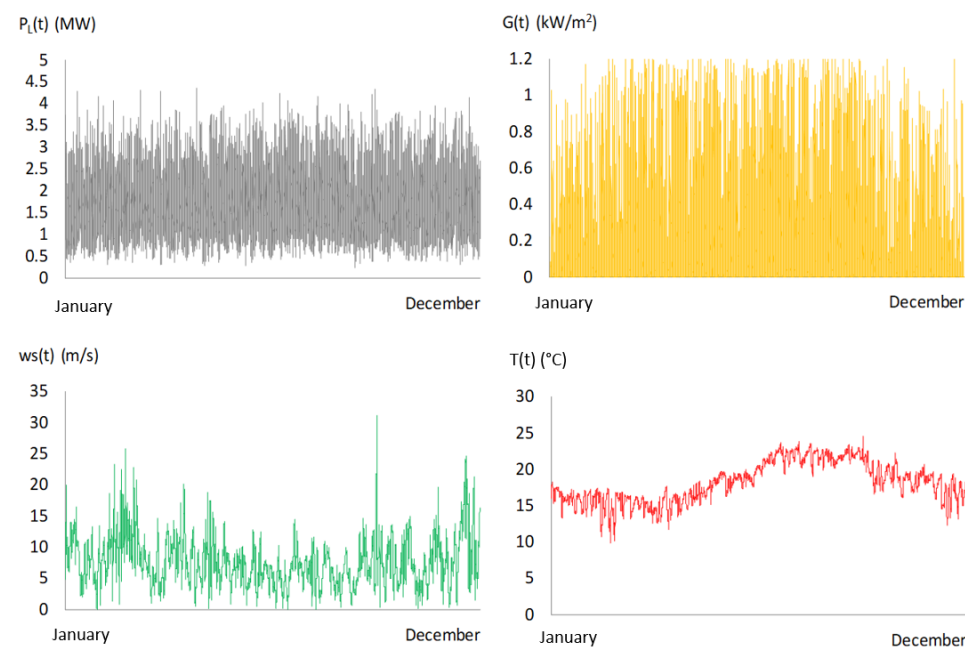


Figure 5. Load, irradiation, wind speed, and temperature over 2019 on Graciosa Island in 15-min steps.

As inverters are grid-forming types (creating the voltage and frequency grid reference), diesel generators must not run all the time; they only supply the net load when it is not supplied by renewables or the battery (load-following strategy).

Table 2 shows the characteristics of the components used in the simulation of Graciosa Island's current system and the optimizations in the next sections. The system lifetime is $Y = 25$ years, the same as the expected lifetimes of the PV and wind turbines. Project management costs plus permits, fees, and indirect costs are expected to be 10% of the system's total CAPEX.

Table 2. Component characteristics.

Variable	Value
Diesel generator CAPEX	84 EUR/kW [52]
Diesel generator OPEX (except fuel)	0.02 EUR/h/kW [42]
Diesel generator lifetime	25,000 h [52]
Diesel fuel cost	1.2074 EUR/L [48]
Diesel fuel cost annual inflation, Inf_{fuel}	3.5% [53]
Diesel fuel emissions, $Em_{D/L}$	3.85 kg CO ₂ -eq/L [54]
PV generator, inc. inverter CAPEX	0.855 EUR/Wac [55]
PV generator annual OPEX	0.5% of CAPEX [56]
NOCT	43 °C [57]
f_{PV_loss}	95% [57]
α	-0.41%/°C [57]
PV inverter DC/AC ratio	1.25 [57]
PV emissions, $Em_{PV/kW}$	1295 kg CO ₂ -eq/kW [54]
Inverter efficiency curve	Variable [58]
Wind turbine CAPEX	1.3 EUR/W [59]
Wind turbine power curve	Figure 2
Wind turbine annual OPEX	2% of CAPEX [59]
Wind turbine emissions, $Em_{WT/kW}$	745.5 kg CO ₂ -eq/kW [60]
LTO battery CAPEX	600 EUR/kWh (market study)
LFP battery CAPEX	200 EUR/kWh (market study)
Battery cost escalation (for replacements)	-4%/yr (limit -60%) [57]
Battery annual OPEX	1% of CAPEX [61]
LFP battery emissions, $Em_{B/kWh}$	76.4 kg CO ₂ -eq/kWh [62]
Inverter-charger CAPEX	160 EUR/kW [63]
Inverter-charger efficiency curve	Variable [58]
Inverter-charger lifetime	15 years
Annual discount rate, I	7%
Annual general inflation rate, Inf	2%
Load required reserve, RR_L	10% [5]
PV required reserve, RR_{PV}	10% [5]
Wind required reserve, RR_W	20% [5]

Simulation results for the current system are shown in Table 3 compared with the GEMS data [48]. Differences in diesel and battery energies could be due to the load time series in 15-min time steps in our study, which have been estimated. Considering the costs shown in Table 1, the NPC of the present system is EUR 65.74 M, with an LCOE of 0.316 EUR/kWh and 236.7 kt of CO₂-eq life cycle emissions.

Table 3. Simulation of Graciosa Island's current energy system.

Results	GEMS	This Study
Load consumption (including losses) (GWh/yr)	14.61	14.63
Diesel supply to load (GWh/yr)	5.70	6.61
PV supply to load (GWh/yr)	0.98	0.99 *
Wind supply to load (GWh/yr)	7.38	7.51 *
Energy stored in battery (GWh/yr)	0.74	0.45
Energy discharged by battery (GWh/yr)	0.58	0.41
Renewable fraction (%)	60.1	54.8
Capacity shortage (%)	**	1.93
NPC (MEUR)	**	65.74
LCOE (EUR/kWh)	**	0.316
LCE (kt of CO ₂ -eq)	**	236.7

* In this study, there is a single AC node where generation, load, and storage are connected. A total annual PV+wind curtailment value of 4.01 GWh/yr was obtained, which was proportionally distributed between the PV and wind generation. ** Data not provided by GEMS ([48]).

4.2. PHS

PHS was considered in the optimization. Near the town of Fontes, there is an elevation where an upper reservoir (359 m above sea level) could be constructed, while a lower reservoir could be near the sea (a location at 77 m above sea level was selected in Figure 6). Therefore, a head difference of more than 280 m could be achieved but 250 m was considered in this study as a conservative value. The distance between the reservoirs is 1600 m.



Figure 6. Possible location of PHS upper and lower reservoirs. Google Earth (2024), Graciosa Island: $39^{\circ}04'01''$ N, $27^{\circ}59'40''$ W. Three-dimensional view [Online]. Available at the following: <https://earth.google.com/web/data=QgIIAEoICOLGx4sGEAA> (accessed on 26 November 2024).

Table 4 shows the PHS data used in the optimization (pump and turbine efficiency in Figure 7). In this case, a reversible pump–turbine machine was considered with the same lifetime as the system. Six possible pump turbine machines were considered (rated power 1 to 6 MW, with a rated flow of 0.5 to 3 m^3/s), with an upper reservoir duration between 2 h and 20 h. The maximum water reservoir considered is $20 \text{ h} \cdot 3 \text{ m}^3/\text{s} \cdot 3600 \text{ s/h} = 216,000 \text{ m}^3$ (considering $H_{LR_max} = 5 \text{ m}$, a square area with 207 m sides would be needed for the reservoir). Carbon steel pipelines are considered in this study (with an absolute roughness of 0.05 mm). To limit pipeline noise and minimize damaging wear and tear on pipes and fittings, the water speed is commonly restricted to a maximum of 2.5 m/s. In this study, the pipeline diameter is calculated based on the rated pump–turbine flow and the 2.5 m/s limit, with a minimum diameter of 600 mm and a maximum diameter of 1500 mm.

Table 4. Components' characteristics.

Variable	Value
Nominal power, $P_{P_N} = P_{HT_N}$	1–6 MW, steps of 1 MW
Nominal flow, $Q_{P_N} = Q_{HT_N}$	0.5–3 m^3/s , steps of 0.5 m^3/s
Pump–turbine CAPEX, inc. civil works	1000 EUR/kW [64]
Reservoir CAPEX	25 EUR/ m^3 [64]
PHS annual OPEX	1.5% of CAPEX [64]
Pump–turbine efficiency curve	Variable [64], Figure 6
Pump–turbine minimum power	20% of nominal power
H_{diff}	250 m
Upper res. duration ($V_{UR_max} = V_{LR_max}$)	2–20 h, steps of 2 h
$V_{UR_min} = V_{LR_min}$	10%
$D_p = D_T$	$0.6 \text{ m} < D_p < 1.5 \text{ m}$, for water speed $< 2.5 \text{ m/s}$
$L_p = L_T$	1600 m
$K_{fittings}$	0.8
ϵ	0.05 mm
$H_{LR_max} = H_{UR_max}$	5 m
PHS emissions, $E_{m_{PHS}/\text{kWh}}$	33 g CO ₂ -eq/kWh [60]

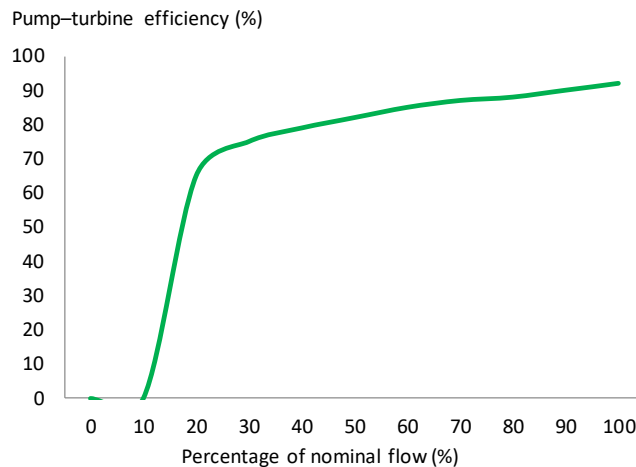


Figure 7. Pump–turbine efficiency.

4.3. Deterministic Optimization

First, a deterministic optimization (without MCS) in 1-h time steps was performed considering the component types and minimum and maximum allowed in parallel (shown in Table 5). The same components as those presented in Table 1 were considered. The presented 4.6 MW diesel genset group and the 7.425 MW inverter–charger group were considered fixed and non-optimizable as they are part of the system and their rated power is enough to supply the maximum load (Figure 5). For the PHS, the components of Table 4 were considered. The constraints were $UL_{\max} = 0\%$ and $RC_{sh,\max\%} = 0\%$.

Table 5. Optimization data and results of the deterministic optimization.

Variables	Types Allowed	Min. and Max. Parallel for Deter. Opt.	Deterministic Optimization Results	Data for Stochastic Optimization
PV_{type} and N_{PV}	1 MWDC	1–12	$1 \text{ MW}_{DC} \times 10 \text{ par.}$	$1 \text{ MW}_{DC}, 6–12$
WT_{type} and N_{WT}	0.9 MW	5–12	$0.9 \text{ MW} \times 5 \text{ par.}$	$0.9 \text{ MW}, 5–8$
D_{type} and N_D		4.6 MW existing diesel genset group (fixed)		
B_{type} and N_B	3.2 MWh (LTO and LFP)	1–5	$3.2 \text{ MWh LFP} \times 3 \text{ par.}$	$3.2 \text{ MWh LFP}, 2–4$
PHS_{type}	1 to 6 MW, steps 1 MW	-	2 MW	1 to 3 MW, steps 1 MW
PHS_{dur}	2 to 20 h, steps 2 h	-	20 h	10 to 20 h, steps 2.5 h

The number of possible combinations of component types and numbers in parallel is $1 \times 12 \times 1 \times 8 \times 1 \times 2 \times 5 \times 6 \times 10 = 57,600$. To optimize the control strategy (vector in Equation (26)) with four setpoint variables, accounting for five possible values for each control variable, the number of possible combinations is $5^4 = 625$. The total combinations (components \times strategies) number 36 million. The computation speed of the computer is 40 simulations (1-h time steps over a whole year) per second; therefore, evaluating all the components would have taken 10.4 days. However, by using GA ($N_{GEN_MAIN_MAX} = 15$; $N_{MAIN} = 400$; $N_{GEN_SEC_MAX} = 10$; $N_{SEC} = 20$; crossover rate 90%; and mutation rate 1% [65]), it took less than 8 h (results of the deterministic optimization are shown in Table 5).

The optimal solution found using the deterministic optimization has an NPC of EUR 34.22 M and an LCOE of 0.162 EUR/kWh, with LFP (much lower cost) instead of LTO batteries. In addition, the setpoints of the optimal combination are as follows:

- $SOC_{max\%} = 100\%$: using all available capacity is optimal, even considering that the high SOC implies higher calendar degradation;
- $SOC_{stp_diesel\%} = 20\%$ (minimum SOC allowed for LFP): charging batteries with diesel is not optimal;
- $P_{HT_prior\%} = 25\%$: if the net load power is lower than 25% of the turbine's rated power, the net load is supplied with a battery—otherwise, the water turbine is used;

- $P_{P_prior\%} = 50\%$: if net renewable power is lower than 50% of the pump's rated power, energy is stored in the battery—otherwise, energy is stored by pumping water.

4.4. Stochastic Optimization

For the stochastic optimization, the variability of the input data is shown in Table 6 (the mean and standard deviation of the load, irradiation, temperature, and wind speed used as PDF data for the MCS approach).

Table 6. Stochastic input variables. Irradiation, load, and temperature obtained from NASA [66] over 39 years (1984–2022).

Variable	Mean	Std. Dev.
L: load (GWh/year)	14.61	0.4 [67]
G: irradiation tilted surface (kWh/m ² /day)	4.53	0.119 [66]
T: temperature (°C)	18.07	0.343 [66]
W: wind speed (m/s)	7.61	0.341 [66]
Inf.F: fuel diesel price annual inflation (%)	3.5	0.3 [53]

The covariance matrix data shown in Equation (33) are detailed in Equation (47). Covariance between G, T, and W was obtained from NASA [66]. Covariances between L and the others were estimated considering a small increase in load consumption due to air conditioning with increased temperatures and irradiation.

$$\Sigma = \begin{bmatrix} 0.1600 & 0.0200 & 0.0200 & 0 \\ 0.0200 & 0.0141 & 0.0242 & -0.0042 \\ 0.0200 & 0.0242 & 0.1161 & -0.0213 \\ 0 & -0.0042 & -0.0213 & 0.1177 \end{bmatrix} \quad (47)$$

The random variation for the values of each time series is $R_{var} = 5\%$.

In the stochastic optimization, to reduce the search space, only $P_{HT_prior\%}$ and $P_{P_prior\%}$ were optimized (maintaining $SOC_{max\%}$ and $SOC_{stp_diesel\%}$, fixed at 100% and 20%, respectively), with possible combinations numbering $5^2 = 25$ (with this low number, no GA was used for the control strategy; all the combinations were evaluated). Considering the deterministic optimization results, we reduced the search space of the main GA for the stochastic optimization to the data in the last column of Table 4, obtaining 31,500 total possible combinations (components × strategies). Considering $MCS_{samples} = 100$ MCSs for each combination of components and control setpoints, the total simulations numbered 3,150,000. With a computing time of seven simulations per second (15-min time steps during a whole year), evaluating all the combinations would take 5.2 days. Using the GA to optimize components ($N_{GEN_MAIN_MAX} = 15$; $N_{MAIN} = 20$ [65]) and evaluate the 25 control strategy combinations, it took less than 15 h (12% of the time required to evaluate all the combinations). The stopping rule maximum standard error considered was $RSE\% = 2\%$.

Detailed results for the optimal system found are shown in Table 7. Only 74 MCSs were performed to find the optimal solution (the stopping rule was met before the maximum of 100 simulations set for the MCS approach was evaluated).

The optimal system obtained by the stochastic optimization includes the same number of wind turbines as the current system; however, it increases PV systems from 1 to 10 MW; the battery is an LFP with double the size of the current one (6.4 MWh) and 3 MW of the PHS; and a 20 h duration is added. With this configuration, the renewable fraction is 96.09% (mean), much higher than in the current system (60%). The optimal control setpoint variables are the same as those of the deterministic optimization. The optimal system includes LFP instead of LTO batteries, and their lifetime was estimated at 10.54 years (mean value of the 74 MCSs).

Table 7. Optimal system obtained with stochastic optimization and its results.

Variable	Values
Optimal system found:	
PV	10 MW _{DC} (1 MW _{DC} × 10 par.)
Wind turbines	4.5 MW (0.9 MW × 5 par.)
Diesel genset (not optimized)	4.6 MW
Battery	6.4 MWh (3.2 MWh × 2, LFP)
Inverter-charger (not optimized)	7.425 MW
Pump-turbine rated power	3 MW
Reservoir capacity and duration	108 dam ³ , 20 h
$P_{HT_prior\%}$	25%
$P_{P_prior\%}$	50%
Simulation results (74 MCSs):	
	Average
Load energy (GWh/yr)	14.82
PV energy (GWh/yr)	13.78
WT energy (GWh/yr)	10.19
Curtailment (GWh/yr)	6.63
Diesel genset energy (GWh/yr)	0.58
Diesel genset fuel consumption (x1E6 L/yr)	0.21
Battery charge energy (GWh/yr)	0.88
Battery discharge energy (GWh/yr)	0.79
Battery lifetime (years)	10.54
Hydro turbine output energy (GWh/yr)	3.15
Pump input energy (GWh/yr)	6.16
Renewable fraction (%)	96.09
Unmet load (%)	0
Life cycle emissions (kt of CO ₂ -eq)	32.5
Capacity shortage (%)	0
NPC (MEUR)	33.83
LCOE (EUR/kWh)	0.160
	Standard dev.
	0.36
	0.32
	0.87
	0.75
	0.16
	0.06
	0.06
	0.05
	0.22
	0.09
	0.15
	1.05
	5.1
	0
	1.33
	0.005

The unmet load and capacity shortage are zero, as required by the constraints. The capacity shortage is zero thanks to the hydro turbine, which runs at a minimum load (20%) during the time steps when the required reserve is lower than the real reserve, providing the needed real reserve (if it is not enough, several diesel generators start to provide the needed real reserve). The NPC (mean, EUR 33.83 M; standard deviation, EUR 1.33 M) and the LCOE (mean 0.160 EUR/kWh; standard deviation, 0.005 EUR/kWh) are much lower than the current system's results (EUR 65.74 M and 0.316 EUR/kWh). Life cycle emissions are much lower at only 13.8% of the current system's emissions (a mean of 32.5 kt of CO₂-eq vs. 236.7 in the current system).

Figure 8 shows the distribution of the costs (NPC mean) and emissions (LCE mean) of the optimal system. More than 50% of life cycle emissions are due to the use of diesel.

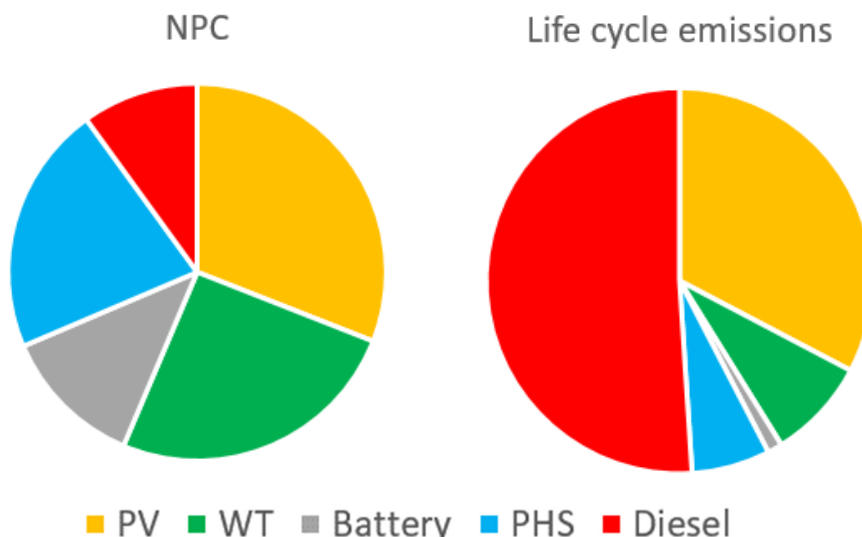
**Figure 8.** NPC and LCE mean distributions of the optimal system.

Figure 9 shows the PDF curves of the input data used in the MCSs of the optimal solution. In all graphs, the Gaussian normal probability density functions that best fit are also shown.

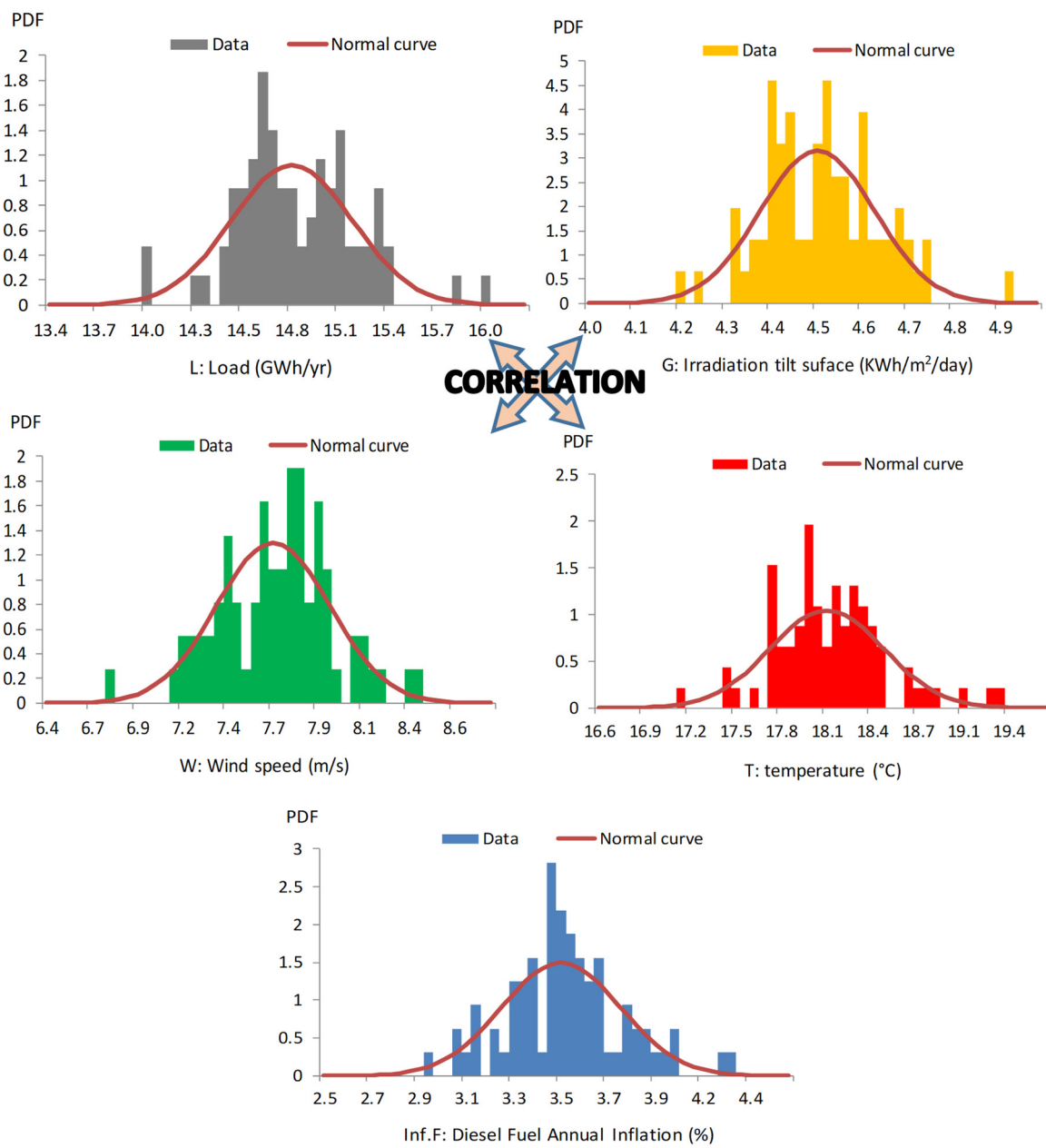


Figure 9. PDFs of the input data used in the optimal system found by the stochastic optimization (74 MCSs until stop rule was reached).

Figure 10 shows that in the 74 MCSs of the optimal system, the NPC varies from EUR 31.7 to 38.1 M (LCOE varies from 0.151 to 0.171). Annual diesel generation is the variable with higher variability, from 0.33 to 1.17 GWh/yr. Battery lifetime varies from 9.85 to 11.15 years.

Figures 11 and 12 show 1 of the 74 MCSs of the optimal system in 15-min time steps over a whole year. The diesel generators only run for a few hours a year. In Figure 12, the net load (+) and net renewable power (−) are shown in the upper graph, and in the same graph, the setpoint limits, $P_{HT_prior\%}$ and $P_{P_prior\%}$, are represented. When the net load is higher than $P_{HT_prior\%}$, the hydro turbine is selected first to supply the net load—otherwise, the batteries discharge. Furthermore, when the net renewable is higher than $P_{P_prior\%}$, energy is stored by pumping water—otherwise, the batteries are charged.

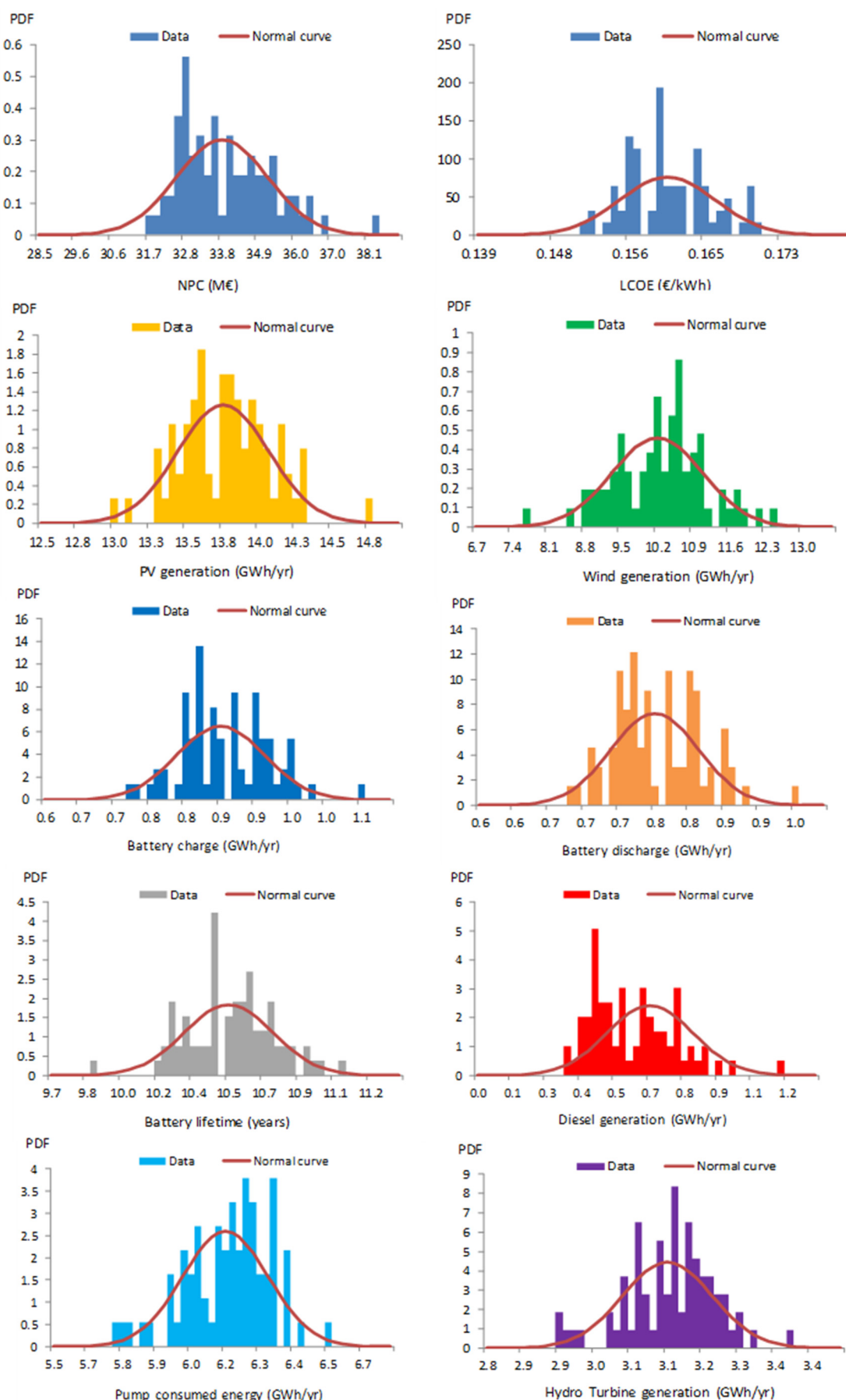


Figure 10. PDFs of the main results of the optimal system found by the stochastic optimization (74 MCSs until stop rule was reached).

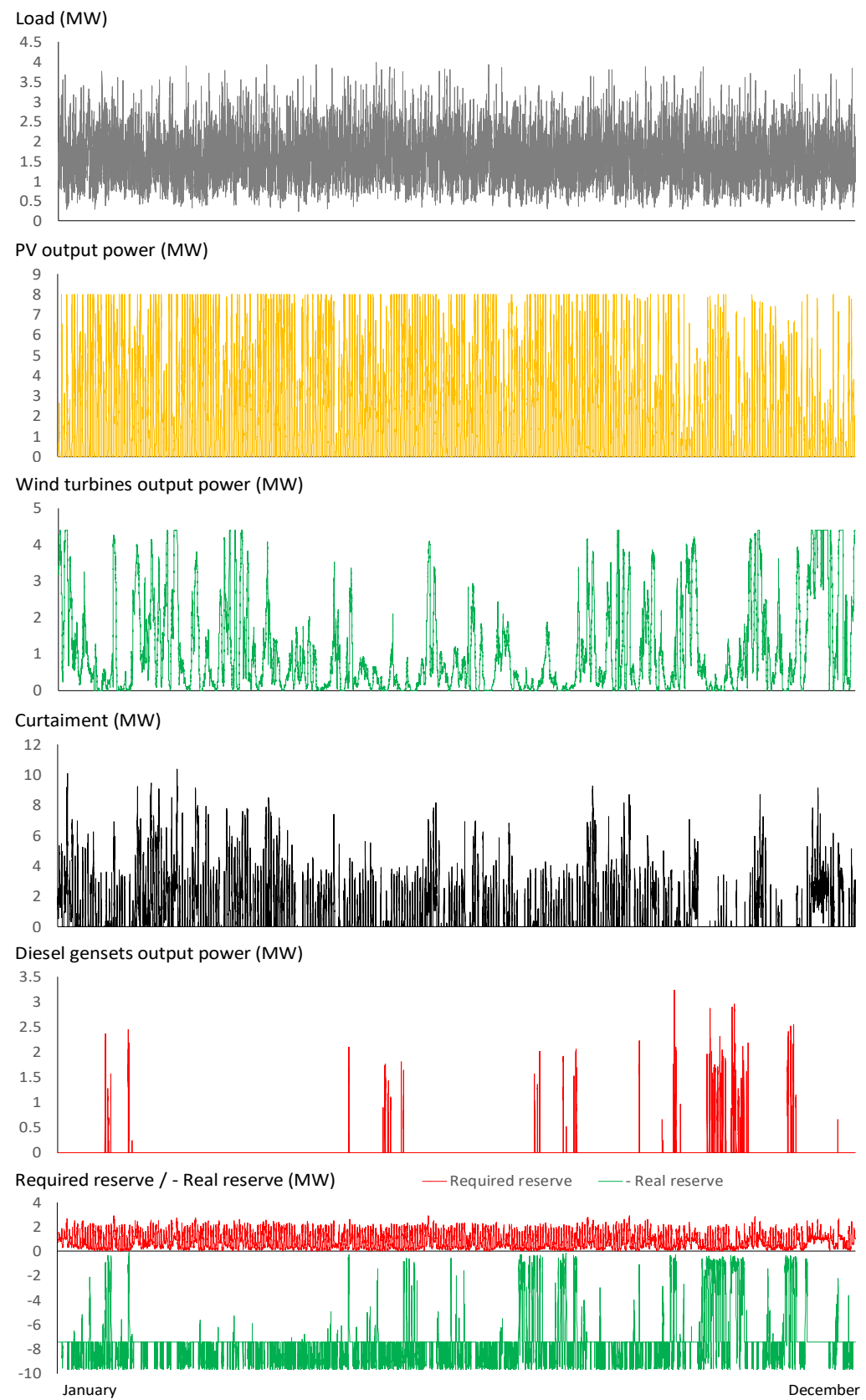


Figure 11. Simulation over a whole year of 1 of the 74 MCSs of the optimal system found by the stochastic optimization.

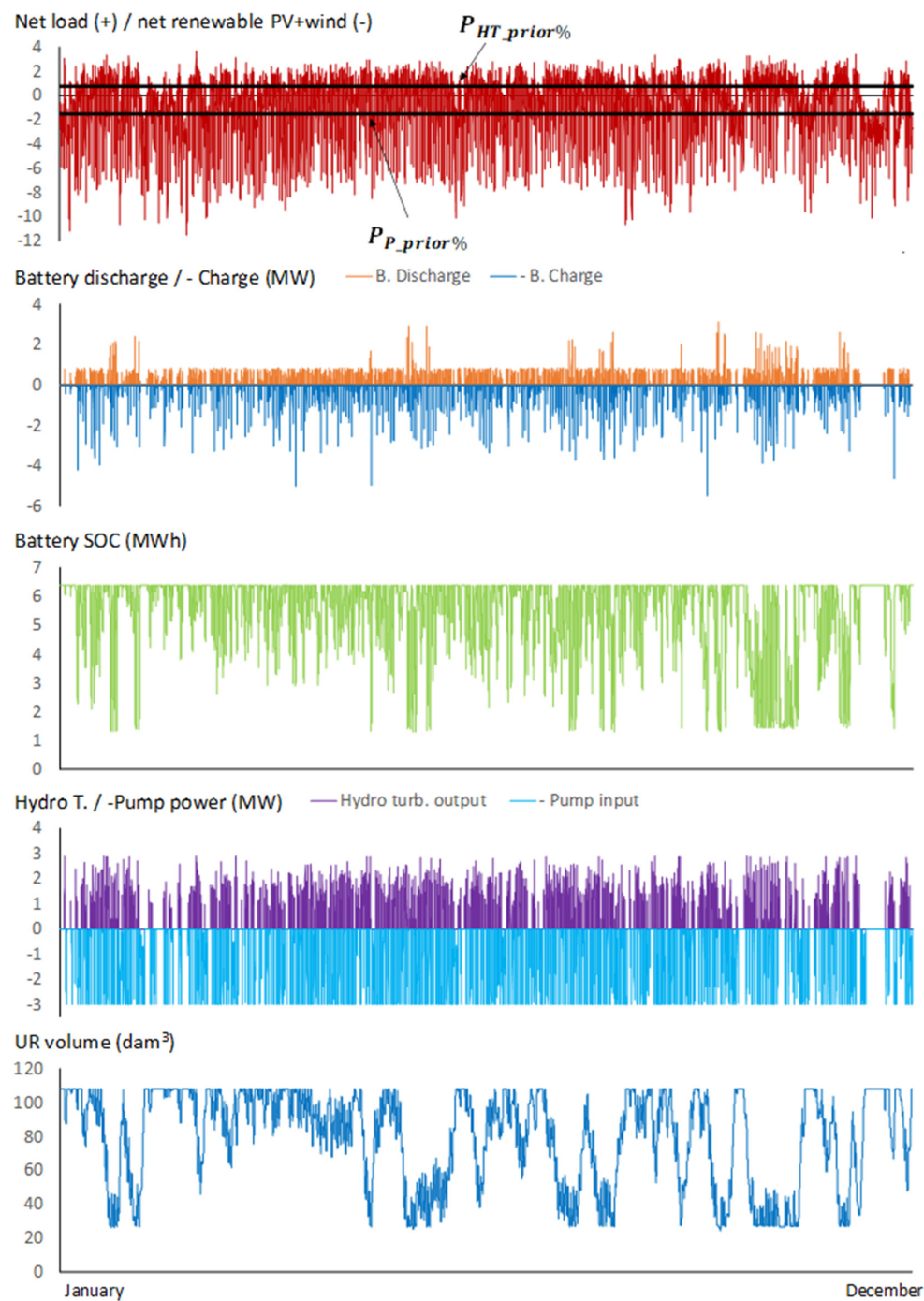


Figure 12. Simulation over a whole year of 1 of the 74 MCSs of the optimal system found by the stochastic optimization (cont.).

4.4.1. Effect on the Average Diesel Fuel Price Inflation

The optimization was performed two more times to observe the effect of different values for the mean of diesel fuel price inflation (1.5 and 2.5%), considering the same standard deviation of 0.3%. The same optimal system was found but the NPC and LCOE values were different. The results are shown in Table 8.

Table 8. Optimal system results for different diesel fuel price inflation mean values.

Mean Fuel Price Inflation (%)	1.5	2.5	3.5
NPC (MEUR) (mean)	32.76	33.19	33.83
LCOE (EUR/kWh) (mean)	0.155	0.157	0.1615

4.4.2. Effect on PHS CAPEX

The effect of the PHS CAPEX on the optimization is shown in Table 9. The optimal system varies with the PHS CAPEX. In the case of high CAPEX (1660 EUR/kW + 56 EUR/m³ [68]), allowing up to eight batteries in parallel in the optimization, the battery size of the optimal system reaches its maximum and no PHS is included in the system. In the case of low CAPEX (547 EUR/kW + 2.7 EUR/m³ [69]), the same optimal system as in the original case is found but with a significantly lower NPC due to the reduced PHS CAPEX. In all cases with hybrid storage, $P_{HT_prior\%}$ = 25% and $P_{P_prior\%}$ = 50%.

Table 9. Optimal system results for different PHS CAPEX values.

PHS CAPEX (EUR/kW + EUR/m ³)	1000 + 25	High [68]: 1660 + 56	Low [69]: 547 + 2.7
Optimal system	PV 10 MW WT 0.9 × 5, Batt. 6.4 MWh + PHS 3 MW, 20 h $P_{HT_prior\%}$, $P_{P_prior\%}$ NPC (MEUR) (mean)	PV 10 MW WT 0.9 × 5 Batt. 25.6 MWh -	PV 10 MW WT 0.9 × 5 Batt. 6.4 MWh + PHS 3 MW, 20 h 25%, 50% 29.32
	33.83	35.41	

4.4.3. Effect on Battery CAPEX

The effect on the battery CAPEX (allowing up to eight batteries in parallel in the optimization) is shown in Table 10. In the case of 100 EUR/kWh, no PHS is included in the optimal system. In all cases with hybrid storage, $P_{HT_prior\%}$ = 25% and $P_{P_prior\%}$ = 50%.

Table 10. Optimal system results for different LFP battery CAPEX.

LFP Battery CAPEX (EUR/kWh)	200	150	100
Optimal system	PV 10 MW WT 0.9 × 5, Batt. 6.4 MWh + PHS 3 MW, 20 h $P_{HT_prior\%}$, $P_{P_prior\%}$ NPC (MEUR) (mean)	PV 10 MW WT 0.9 × 5, Batt. 12.8 MWh + PHS 2 MW, 20 h 25%, 50% 32.70	PV 10 MW WT 0.9 × 5 Batt. 25.6 MWh -
	33.83		31.17

4.4.4. GA Statistical Test Results

The stochastic optimization has been repeated $R = 20$ times (using the same MCS data) to obtain statistical results of the GA's behavior. Figure 13 shows the evolution of the NPC (mean) over the generations in the different executions, while Table 11 presents the statistical results. In total, 16 out of the 20 runs obtained the global optimum.

Table 11. Statistical results of the optimization techniques.

Variable	GA	PSO
SD_{opt} (MEUR)	0.0898	0.0655
RLE_{opt}	0.0238	0.0136
MAE_{opt} (MEUR)	0.0404	0.0230
$RMSE_{opt}$ (MEUR)	0.0964	0.0679
η_{opt} (%)	98.82	99.93
Average execution time (h)	14.7	13.9

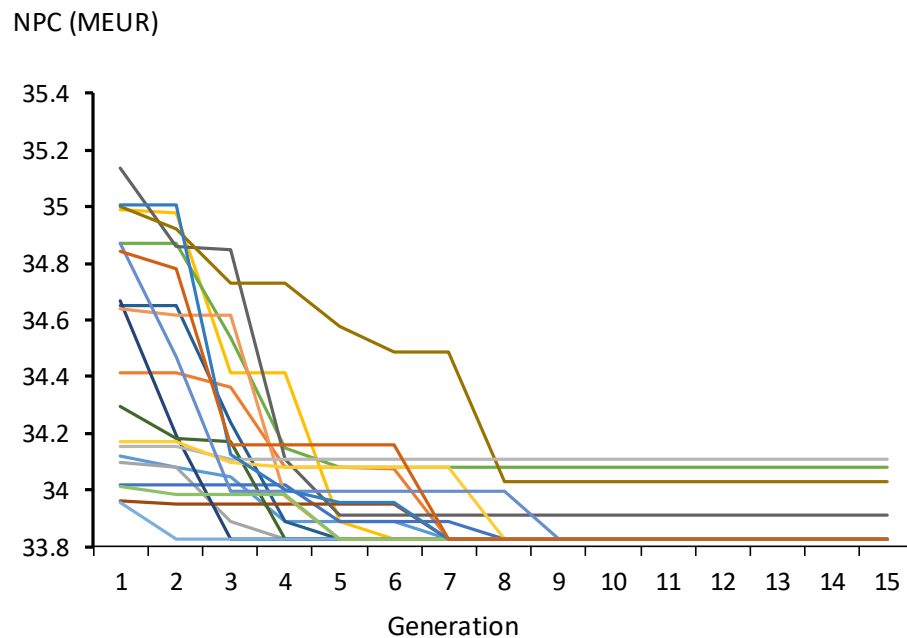


Figure 13. GA. Evolution of the NPC, with each color representing one of the twenty runs.

4.4.5. Results Comparison Using an Alternative Metaheuristic Technique (PSO)

For comparison purposes, the optimization was performed using a discrete version of the PSO algorithm [70] instead of the main GA. PSO parameters were (similar to the GA) as follows: number of iterations = 15; population size = 20; cognitive coefficient = 2; social coefficient = 2; and inertia weight = 0.5. Figure 14 shows the evolution of the NPC (mean) over the generations in the different executions. The statistical results of the PSO are presented in the last column of Table 11 (in this case, the PSO results are slightly better than the GA results). In total, 17 out of the 20 runs obtained the global optimum.

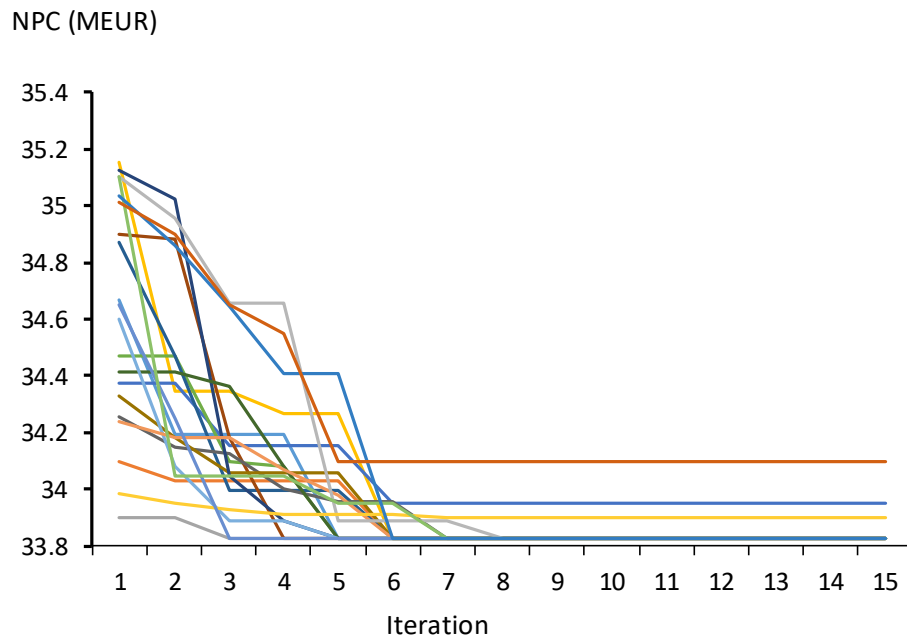


Figure 14. PSO. Evolution of the NPC, with each color representing one of the twenty runs.

5. Conclusions

This study presented a metaheuristic–stochastic optimization using genetic algorithms and Monte Carlo simulations of a stand-alone hybrid system that can comprise PV, wind

turbines, diesel gensets, battery banks, and/or PHS. The sizes of the components and the control setpoints were optimized. Unlike previous optimization research, the system simulation was performed with high accuracy, considering the variable efficiency of the components (inverters, pumps, and turbines), the PHS variable losses and variable head, and battery lifetime prediction (taking into account cycling and calendar degradation). The variability and correlation of wind speed, irradiation, temperature, load, and diesel fuel price inflation were considered using the probabilistic approach. The hybrid PHS–battery storage was controlled by setpoint variables (limits on using PHS or battery to supply or store energy), which were optimized. Furthermore, the maximum battery SOC and the SOC setpoint for battery charging using diesel gensets (when they are run) were optimized.

The simulation and optimization model (implemented in C++) is validated by comparing it to previous research by other authors (which used Matlab, <https://www.mathworks.com/products/matlab.html>). In addition, it was found that the calculation speed of our model is more than 100 times faster than that of previous research, allowing the stochastic optimization to be performed in a similar amount of time as other studies that use deterministic optimization.

The optimization was applied to Graciosa Island (Portugal), obtaining an optimal system that includes hybrid PHS–battery storage. Compared with the current system, this optimal system has a much lower NPC and LCOE (roughly 50% of the current system values), much higher renewable penetration (96% vs. 57%), much lower life cycle emissions (roughly 14% of the current system emissions), and zero reserve capacity shortage. In this case, the optimal setpoint to select the PHS or the battery during charge is 50% of the nominal pump power (if net renewable power is lower than 50% of the pump’s rated power, energy is stored in the battery—otherwise, energy is stored by pumping). During discharge, the optimal setpoint is 25% of the nominal turbine power (if the net load power is lower than 25% of the turbine’s rated power, the net load is supplied with the battery—otherwise, the water turbine is used). The optimal maximum SOC is 100% (the optimal control uses all the available battery capacity, even considering that a high SOC implies higher calendar degradation). The SOC setpoint to charge the battery when the diesel gensets are running is the minimum SOC; that is, it is not worthwhile to charge the battery with diesel. The optimal sizes and setpoints could be different for other applications (different locations, component characteristics, loads, costs, etc.) so it is necessary to perform the optimization for each case. Several sensitivity analyses have been performed in the optimization of Graciosa Island. Diesel fuel inflation has a low effect on the optimization as the diesel generator operates for only a few hours each year. Both the PHS CAPEX and the battery CAPEX have a significant effect on the optimization—with high PHS CAPEX (1660 EUR/kW + 56 EUR/m³) or low LFP battery CAPEX (100 EUR/kWh), the optimal solution consists of battery storage only, with no PHS included.

Author Contributions: Conceptualization, R.D.-L.; methodology, R.D.-L.; software, R.D.-L. and J.M.L.-R.; validation, R.D.-L. and J.M.L.-R.; formal analysis, R.D.-L. and J.M.L.-R.; investigation, R.D.-L.; resources, R.D.-L.; data curation, J.M.L.-R.; writing—original draft preparation, R.D.-L.; writing—review and editing, J.M.L.-R.; visualization, R.D.-L.; supervision, R.D.-L.; project administration, R.D.-L.; funding acquisition, R.D.-L. All authors have read and agreed to the published version of the manuscript.

Funding: This study was supported by the Spanish Government (Ministerio de Ciencia e Innovación, Agencia Estatal de Investigación), the European Union [Grant No. TED2021-129801B-I00 funded by MCIN/AEI/10.13039/501100011033 and the European Union NextGenerationEU/PRTR], and the European Regional Development Fund [Grant PID2021-123172OB-I00 funded by MCIN/AEI/10.13039/501100011033 and by “ERDF A way of making Europe”].

Data Availability Statement: The data are available at <https://doi.org/10.5281/zenodo.14260577> (accessed on 9 January 2025).

Conflicts of Interest: The authors declare that there are no conflicts of interest regarding the publication of this study.

References

1. Moosavian, S.F.; Noorollahi, Y.; Shoaei, M. Renewable energy resources utilization planning for sustainable energy system development on a stand-alone island. *J. Clean. Prod.* **2024**, *439*, 140892. [[CrossRef](#)]
2. Eras-Almeida, A.A.; Egido-Aguilera, M.A. Hybrid renewable mini-grids on non-interconnected small islands: Review of case studies. *Renew. Sustain. Energy Rev.* **2019**, *116*, 109417. [[CrossRef](#)]
3. Barney, A.; Polatidis, H.; Jelić, M.; Tomasević, N.; Pillai, G.; Haralambopoulos, D. Transition towards decarbonisation for islands: Development of an integrated energy planning platform and application. *Sustain. Energy Technol. Assess.* **2021**, *47*, 101501. [[CrossRef](#)]
4. Fotopoulou, M.; Pediaditis, P.; Skopetou, N.; Rakopoulos, D.; Christopoulos, S.; Kartalidis, A. A Review of the Energy Storage Systems of Non-Interconnected European Islands. *Sustainability* **2024**, *16*, 1572. [[CrossRef](#)]
5. Groppi, D.; Feijoo, F.; Pfeifer, A.; Garcia, D.A.; Duic, N. Analyzing the impact of demand response and reserves in islands energy planning. *Energy* **2023**, *278*, 127716. [[CrossRef](#)]
6. Schierhorn, P.; Turnell, A.V.; Masendorf, D.; Ackermann, T. High Penetration of PV in Tropical Island Systems Experiences from Indonesia. In Proceedings of the 4th International Hybrid Power Systems Workshop, Crete, Greece, 22–23 May 2019.
7. Schömann, O.; Sadri, H.; Krüger, W.; Bülo, T.; Hardt, C.; Hesse, R.; Falk, A.; Stankat, P.R. Experience with Large Grid-Forming Inverters on Various Island and Microgrid Projects. In Proceedings of the 4th International Hybrid Power Systems Workshop, Crete, Greece, 22–23 May 2019.
8. Blakers, A.; Stocks, M.; Lu, B.; Cheng, C.; Stocks, R. Pathway to 100% Renewable Electricity. *IEEE J. Photovolt.* **2019**, *9*, 1828–1833. [[CrossRef](#)]
9. Javed, M.S.; Ma, T.; Jurasz, J.; Amin, M.Y. Solar and wind power generation systems with pumped hydro storage: Review and future perspectives. *Renew. Energy* **2020**, *148*, 176–192. [[CrossRef](#)]
10. Rehman, S.; Al-Hadhrami, L.M.; Alam, M.M. Pumped hydro energy storage system: A technological review. *Renew. Sustain. Energy Rev.* **2015**, *44*, 586–598. [[CrossRef](#)]
11. Latorre, F.J.G.; Quintana, J.J.; de la Nuez, I. Technical and economic evaluation of the integration of a wind-hydro system in El Hierro island. *Renew. Energy* **2019**, *134*, 186–193. [[CrossRef](#)]
12. Al Katsaprakakis, D.; Thomsen, B.; Dakanali, I.; Tzirakis, K. Faroe Islands: Towards 100% R.E.S. penetration. *Renew. Energy* **2019**, *135*, 473–484. [[CrossRef](#)]
13. Papaefthymiou, S.V.; Karamanou, E.G.; Papathanassiou, S.A.; Papadopoulos, M.P. A wind-hydro-pumped storage station leading to high RES penetration in the autonomous island system of Ikaria. *IEEE Trans. Sustain. Energy* **2010**, *1*, 163–172. [[CrossRef](#)]
14. Cavazzini, G.; Benato, A.; Pavese, G.; Ardizzon, G. Techno-economic benefits deriving from optimal scheduling of a Virtual Power Plant: Pumped hydro combined with wind farms. *J. Energy Storage* **2021**, *37*, 102461. [[CrossRef](#)]
15. Gioutsos, D.M.; Blok, K.; van Velzen, L.; Moorman, S. Cost-optimal electricity systems with increasing renewable energy penetration for islands across the globe. *Appl. Energy* **2018**, *226*, 437–449. [[CrossRef](#)]
16. Rodrigues, A.; Machado, D.; Dentinho, T. Electrical energy storage systems feasibility; The case of Terceira Island. *Sustainability* **2017**, *9*, 1276. [[CrossRef](#)]
17. Kotb, K.M.; Elkadeem, M.R.; Khalil, A.; Imam, S.M.; Hamada, M.A.; Sharshir, S.W.; Dán, A. A fuzzy decision-making model for optimal design of solar, wind, diesel-based RO desalination integrating flow-battery and pumped-hydro storage: Case study in Baltim, Egypt. *Energy Convers. Manag.* **2021**, *235*, 113962. [[CrossRef](#)]
18. Shabani, M.; Dahlquist, E.; Wallin, F.; Yan, J. Techno-economic comparison of optimal design of renewable-battery storage and renewable micro pumped hydro storage power supply systems: A case study in Sweden. *Appl. Energy* **2020**, *279*, 115830. [[CrossRef](#)]
19. Serat, Z. Optimizing renewable energy systems for 100% clean energy target: A comparative study of solar, hydro, pumped hydro, and battery storage technologies. *J. Energy Storage* **2024**, *104*, 114441. [[CrossRef](#)]
20. Al Katsaprakakis, D. Toward a Renewable and Sustainable Energy Pattern in Non-Interconnected Rural Monasteries: A Case Study for the Xenofontos Monastery, Mount Athos. *Sustainability* **2024**, *16*, 2111. [[CrossRef](#)]
21. Ali, S.; Jang, C.M. Optimum design of hybrid renewable energy system for sustainable energy supply to a remote Island. *Sustainability* **2020**, *12*, 1280. [[CrossRef](#)]
22. Alturki, F.A.; Awwad, E.M. Sizing and cost minimization of standalone hybrid wt/pv/biomass/pump-hydro storage-based energy systems. *Energies* **2021**, *14*, 489. [[CrossRef](#)]

23. Madeira Electricity Supply, (n.d.). Available online: <http://insulae-h2020.eu/pilots/lighthouse-island-3-madeira/> (accessed on 21 November 2024).
24. Siemens, Siemens e Fluence Apoiam a Transição Energética da Ilha da Madeira e Aumentam a Resiliência da Sua Rede Elétrica, (n.d.). Available online: <https://press.siemens.com/pt/pt/comunicadodeimprensa/siemens-e-fluence-apoiam-transicao-energetica-da-ilha-da-madeira-e-aumentam> (accessed on 21 November 2024).
25. Schreider, A.; Bucher, R. An auspicious combination: Fast-ramping battery energy storage and high-capacity pumped hydro. *Energy Procedia* **2018**, *155*, 156–164. [CrossRef]
26. Bertsou, M.M.; Baltas, E. Integration of Different Storage Technologies towards Sustainable Development—A Case Study in a Greek Island. *Wind* **2024**, *4*, 68–89. [CrossRef]
27. Yadav, S.; Kumar, P.; Kumar, A. Grey wolf optimization based optimal isolated microgrid with battery and pumped hydro as double storage to limit excess energy. *J. Energy Storage* **2023**, *74*, 109440. [CrossRef]
28. Javed, M.S.; Ma, T.; Jurasz, J.; Ahmed, S.; Mikulik, J. Performance comparison of heuristic algorithms for optimization of hybrid off-grid renewable energy systems. *Energy* **2020**, *210*, 118599. [CrossRef]
29. Guezgouz, M.; Jurasz, J.; Bekkouche, B.; Ma, T.; Javed, M.S.; Kies, A. Optimal hybrid pumped hydro-battery storage scheme for off-grid renewable energy systems. *Energy Convers. Manag.* **2019**, *199*, 112046. [CrossRef]
30. Bhayo, B.A.; Al-Kayiem, H.H.; Gilani, S.I.U.; Ismail, F.B. Power management optimization of hybrid solar photovoltaic-battery integrated with pumped-hydro-storage system for standalone electricity generation. *Energy Convers. Manag.* **2020**, *215*, 112942. [CrossRef]
31. Ma, T.; Yang, H.; Lu, L. Feasibility study and economic analysis of pumped hydro storage and battery storage for a renewable energy powered island. *Energy Convers. Manag.* **2014**, *79*, 387–397. [CrossRef]
32. Toufani, P.; Karakoyun, E.C.; Nadar, E.; Fosso, O.B.; Kocaman, A.S. Optimization of pumped hydro energy storage systems under uncertainty: A review. *J. Energy Storage* **2023**, *73*, 109306. [CrossRef]
33. Dufo-López, R. Software iHOGA/MHOGA. 2023. Available online: <https://ihoga.unizar.es/en/> (accessed on 5 May 2023).
34. González-Longatt, F.; Wall, P.P.; Terzija, V. Wake effect in wind farm performance: Steady-state and dynamic behavior. *Renew. Energy* **2012**, *39*, 329–338. [CrossRef]
35. Armand, M.; Axmann, P.; Bresser, D.; Copley, M.; Edström, K.; Ekberg, C.; Guyomard, D.; Lestriez, B.; Novák, P.; Petranikova, M.; et al. Lithium-ion batteries—Current state of the art and anticipated developments. *J. Power Sources* **2020**, *479*, 228708. [CrossRef]
36. Itani, K.; De Bernardinis, A. Review on New-Generation Batteries Technologies: Trends and Future Directions. *Energies* **2023**, *16*, 7530. [CrossRef]
37. Naumann, M.; Spingler, F.; Jossen, A. Analysis and modeling of cycle aging of a commercial LiFePO₄/graphite cell. *J. Power Sources* **2020**, *451*, 227666. [CrossRef]
38. Naumann, M.; Schimpe, M.; Keil, P.; Hesse, H.C.; Jossen, A. Analysis and modeling of calendar aging of a commercial LiFePO₄/graphite cell. *J. Energy Storage* **2018**, *17*, 153–169. [CrossRef]
39. Stroe, A.I.; Stroe, D.L.; Knap, V.; Swierczynski, M.; Teodorescu, R. Accelerated Lifetime Testing of High Power Lithium Titanate Oxide Batteries. In Proceedings of the 2018 IEEE Energy Conversion Congress and Exposition (ECCE), Portland, OR, USA, 23–27 September 2018; pp. 3857–3863. [CrossRef]
40. Mousavi, N.; Kothapalli, G.; Habibi, D.; Khiadani, M.; Das, C.K. An improved mathematical model for a pumped hydro storage system considering electrical, mechanical, and hydraulic losses. *Appl. Energy* **2019**, *247*, 228–236. [CrossRef]
41. Skarstein, O.; Uhlen, K. Design Considerations with Respect to Long-Term Diesel Saving in Wind/Diesel Plants. *Wind. Eng.* **1989**, *13*, 72–87.
42. Matt, C.F.; Vieira, L.S.R.; Soares, G.F.W.; De Faria, L.P.T. Optimization of the Operation of Isolated Industrial Diesel Stations. In Proceedings of the 6th World Congress on Structural and Multidisciplinary Optimization, Rio de Janeiro, Brazil, 30 May–3 June 2005.
43. Akbas, B.; Kocaman, A.S.; Nock, D.; Trotter, P.A. Rural electrification: An overview of optimization methods. *Renew. Sustain. Energy Rev.* **2022**, *156*, 111935. [CrossRef]
44. Kenney, J.; Keeping, E.S. *Mathematics of Statistics*; Van Nostrand: New York, NY, USA, 1963.
45. Everitt, B.S. *The Cambridge Dictionary of Statistics*; Cambridge University Press: Cambridge, UK, 2003.
46. Gilli, M.; Maringe, D.; Schumann, E. *Numerical Methods and Optimization in Finance*; Academic Press: Cambridge, MA, USA, 2011.
47. Pfenninger, S.; Staffell, I. Renewable Ninja. 2020. Available online: <https://www.renewables.ninja> (accessed on 20 March 2023).
48. Nogueira, T.; Jesus, J.; Magano, J. Graciosa Island’s Hybrid Energy System Expansion Scenarios: A Technical and Economic Analysis. *J. Sustain. Res.* **2024**, *6*, e2400010. [CrossRef]
49. Stenzel, P.; Schreiber, A.; Marx, J.; Wulf, C.; Schreieder, M.; Stephan, L. Environmental impacts of electricity generation for Graciosa Island, Azores. *J. Energy Storage* **2018**, *15*, 292–303. [CrossRef]
50. Conde, D.; Graciólica, S.; Santa Cruz Da Graciosa, L.; Taveira, N. The hybrid power plant in Graciosa island—a pioneer project in the Azores islands. In Proceedings of the 6th Hybrid Power Systems Workshop, Madeira, Portugal & Virtually, 26–27 April 2022; pp. 26–27.

51. European Commission. PVGIS. 2020. Available online: <https://ec.europa.eu/jrc/en/pvgis> (accessed on 20 March 2023).
52. Lavrik, A.; Zhukovskiy, Y.; Tcvetkov, P. Optimizing the size of autonomous hybrid microgrids with regard to load shifting. *Energies* **2021**, *14*, 5059. [CrossRef]
53. Historical Diesel Price Portugal, (n.d.). Available online: https://es.globalpetrolprices.com/Portugal/diesel_prices/ (accessed on 2 November 2024).
54. United Nations. Life Cycle Assessment of Electricity Generation Options. *United Nations Economic Comission for Europe, Geneva*, 2021. Available online: https://unece.org/sites/default/files/2021-11/LCA_final.pdf (accessed on 17 October 2024).
55. Ramasamy, V.; Zuboy, J.; Shaughnessy, E.O.; Feldman, D.; Desai, J.; Woodhouse, M.; Basore, P.; Margolis, R.; Ramasamy, V.; Zuboy, J.; et al. U.S. Solar Photovoltaic System and Energy Storage Cost Benchmarks, with Minimum Sustainable Price Analysis: Q1 2022. 2022. Available online: <https://www.nrel.gov/docs/fy22osti/83586.pdf#:~:text=For%20this%20Q1%202022%20report,%20we%20introduce%20new,short-term%20distortions%20caused%20by%20policy%20and%20market%20eve> (accessed on 17 October 2024).
56. Bolinger, M.; Seel, J.; Warner, C.; Robson, D. *Utility-Scale Solar*; 2022 Edition; Berkeley Lab: Berkeley, CA, USA, 2022.
57. Dufo-López, R.; Lujano-Rojas, J.M.; Artal-Sevil, J.S.; Bernal-Agustín, J.L. Optimising Grid-Connected PV-Battery Systems for Energy Arbitrage and Frequency Containment Reserve. *Batteries* **2024**, *10*, 427. [CrossRef]
58. DiOrio, N.; Denholm, P.; Hobbs, W.B. A model for evaluating the configuration and dispatch of PV plus battery power plants. *Appl. Energy* **2020**, *262*, 114465. [CrossRef]
59. Wiser, R.; Bolinger, M.; Hoen, B. Land-Based Wind Market Report: 2022 Edition. 2022; pp. 1–91. Available online: <https://www.energy.gov/eere/wind/articles/land-based-wind-market-report-2022-edition> (accessed on 12 September 2024).
60. Nicholson, S.; Heath, G. *Life Cycle Greenhouse Gas Emissions from Electricity Generation*; National Renewable Energy Laboratory: Golden, CO, USA, 2021; p. 3. Available online: <https://data.nrel.gov/submissions/171> (accessed on 12 September 2024).
61. Asian Development Bank. *Handbook on battery Energy Storage*; Asian Development Bank: Metro Manila, Philippines, 2018.
62. Quan, J.; Zhao, S.; Song, D.; Wang, T.; He, W.; Li, G. Comparative life cycle assessment of LFP and NCM batteries including the secondary use and different recycling technologies. *Sci. Total Environ.* **2022**, *819*, 153105. [CrossRef] [PubMed]
63. Ramasamy, V.; Zuboy, J.; Woodhouse, M.; O'Shaughnessy, E.; Feldman, D.; Desai, J.; Walker, A.; Margolis, R.; Basore, P. *U.S. Solar Photovoltaic System and Energy Storage Cost Benchmarks, with Minimum Sustainable Price Analysis: Q1 2023*; National Renewable Energy Laboratory: Golden, CO, USA, 2023. Available online: <https://www.nrel.gov/docs/fy23osti/87303.pdf> (accessed on 12 September 2024).
64. Dufo-López, R.; Lujano-Rojas, J.M. Simulation and Optimisation of Utility-Scale PV-Wind Systems with Pumped Hydro Storage. *Appl. Sci.* **2024**, *14*, 7033. [CrossRef]
65. Bernal-Agustín, J.L.; Dufo-López, R. Efficient design of hybrid renewable energy systems using evolutionary algorithms. *Energy Convers. Manag.* **2009**, *50*, 479–489. [CrossRef]
66. National Aeronautics and Space Administration, NASA POWER Prediction of Worldwide Energy Resources. 2023. Available online: <https://Power.Larc.Nasa.Gov/> (accessed on 13 May 2023).
67. Dufo-López, R.; Cristóbal-Monreal, I.R.; Yusta, J.M. Stochastic-Heuristic Methodology for the Optimisation of Components and Control Variables of PV-Wind-Diesel-Battery Stand-Alone Systems. *Renew. Energy* **2016**, *99*, 919–935. [CrossRef]
68. Mongird, K.; Viswanathan, V.; Alam, J.; Vartanian, C.; Sprenkle, V.; Baxter, R. 2020 Grid Energy Storage Technology Cost and Performance Assessment. *Energy*. 2020. Available online: https://www.pnnl.gov/sites/default/files/media/file/PSH_Methodology_0.pdf (accessed on 12 September 2024).
69. Nassar, Y.F.; Abdunnabi, M.J.; Sbeta, M.N.; Hafez, A.A.; Amer, K.A.; Ahmed, A.Y.; Belgasim, B. Dynamic analysis and sizing optimization of a pumped hydroelectric storage-integrated hybrid PV/Wind system: A case study. *Energy Convers. Manag.* **2021**, *229*, 113744. [CrossRef]
70. Papazoglou, G.; Biskas, P. Review and Comparison of Genetic Algorithm and Particle Swarm Optimization in the Optimal Power Flow Problem. *Energies* **2023**, *16*, 1152. [CrossRef]

Disclaimer/Publisher's Note: The statements, opinions and data contained in all publications are solely those of the individual author(s) and contributor(s) and not of MDPI and/or the editor(s). MDPI and/or the editor(s) disclaim responsibility for any injury to people or property resulting from any ideas, methods, instructions or products referred to in the content.